Synthesis and Reactivity of Diiminopyridine and Iminopyridine Cobalt Complexes

by

Matthew Ray Mena

A Thesis Presented in Partial Fulfillment
of the Requirements for the Degree
Master of Science

Approved May 2021 by the
Graduate Supervisory Committee

Ryan J. Trovitch, Chair
Anne K. Jones
Laura K. G. Ackerman

ARIZONA STATE UNIVERSITY

May 2021

ABSTRACT

Alkylphosphine- and alkylpyridine-substituted 2,6-bis(imino)pyridines (pyridine diimines, PDI) have recently been used as polydentate, redox non-innocent ligands that support the development of highly active catalysts. The alkyl phosphine-substituted ligand, ^{Ph2PPr}PDI, was added to $(Ph_3P)_3CoCl$ and subsequent reduction using excess sodium amalgam yielded (^{Ph2PPr}PDI)Co. Electronic structure analysis revealed a cobalt(I) complex that features a singly reduced PDI chelate. Additionally, low valent ^{Ph2PPr}PDI complexes of Fe and Ni were synthesized and structurally characterized. Furthermore, a series of ^{Ph2PPr}PDI Mn, Fe, Co, and Ni complexes were investigated to evaluate ligand denticity and redox activity. Finally, the catalytic hydrosilylation of carbonyls was investigated to compare the activity of the series and determine whether electron count plays a role in catalysis.

An analogous ligand system featuring alkylpyridine substituents, ^{PyEt}PDI, was added to $CoCl_2$, affording a cobalt dichloride complex with the formula [(^{PyEt}PDI)CoCl][Cl]. Single crystal X-ray diffraction revealed a high-spin cobalt(II) center that possesses an octahedral geometry and an outer-sphere chloride ion. Further treatment using 2 equivalents of $NaEt_3BH$ resulted in the formation of (κ^4-*N*,*N*,*N*,*N*-^{PyEt}IP^{CHMe}N^{EtPy})Co, which has been verified by multinuclear NMR spectroscopy and single crystal X-ray diffraction. (κ^4-*N*,*N*,*N*,*N*-^{PyEt}IP^{CHMe}N^{EtPy})Co was then used in the catalytic hydroboration of nitriles at ambient conditions to yield the corresponding *N*,*N*-diborylamines, which were used as precursors for amide formation.

For:

Ray Mena

Maria Guadalupe Arreola

Crawford

ACKNOWLEDGMENTS

Foremost, I would like to express my sincere gratitude to my advisor Prof. Ryan J. Trovitch for continuous support in my studies and research, for his patience, actionable advice, motivation, and immense knowledge. His guidance helped me grow and develop as an independent scientist every step of the way as a graduate student; I could not have imagined a better advisor and mentor.

Besides my advisor, I must also acknowledge my thesis committee: Prof. Anne K. Jones and Prof. Laura K. G. Ackerman for their encouragement and direction by asking challenging questions during my time here. Prof. Trovitch, Prof. Jones, and Prof. Ackerman exude expansive knowledge; something I hope to one day possess and it has been critical in my development to visualize what it takes to become an independent researcher at a top university.

This would not have been possible without my group members: Thu Thao Nguyen and Anuja Sharma. They were the backbone of my development, contributing in ways much more impactful than independent thinking would have taken me. I will always be indebted to them for being a beacon of support and will forever cherish the moments we had in and out of the lab.

I would also like to acknowledge Dr. Brian Cherry, Dr. Samrat Amin, Dr. Thomas Groy, Brock Leland, Dr. Marco Flores, and Dr. Mu-Hyun Baik and his group for their guidance and assistance.

TABLE OF CONTENTS

CHAPTER Page

LIST OF TABLES

Table Page

LIST OF FIGURES

Figure Page

Figure Page

CHAPTER 1 – SYNTHESIS AND REACTIVITY OF A κ^5-BIS(IMINO)PYRIDINE COBALT COMPLEX AND THE IMPORTANCE OF ELECTRON COUNT IN FIRST ROW METAL CATALYSIS

1.1 Abstract

A series of Fe, Co, and Ni bis(imino)pyridine complexes have been prepared by treating the corresponding metal precursors with ligand followed by sodium amalgam reduction. The addition of ^{Ph2PPr}PDI to $FeBr_2$ resulted in the formation of [(^{Ph2PPr}PDI)FeBr][Br]. Reduction of this precursor yielded (^{Ph2PPr}PDI)Fe, which has been found to have a low-spin Fe(II) center. Similarly, the addition of ^{Ph2PPr}PDI to $(Ph_3P)_3CoCl$ resulted in the formation of [(^{Ph2PPr}PDI)Co][Cl], and further reduction using sodium amalgam afforded (^{Ph2PPr}PDI)Co. Electron paramagnetic resonance spectroscopy and density functional theory calculations confirmed that this compound features an $S = 1/2$ Co center. Lastly, addition of ^{Ph2PPr}PDI to $Ni(COD)_2$ resulted in the formation of (^{Ph2PPr}PDI)Ni, which features a highly distorted square planar geometry about the Ni center. EPR characterization revealed that (^{Ph2PPr}PDI)Ni possesses uncoupled Ni and PDI based electrons. Following their synthesis, the benzaldehyde and acetophenone hydrosilylation activity of (^{Ph2PPr}PDI)Mn, (^{Ph2PPr}PDI)Fe, (^{Ph2PPr}PDI)Co, and (^{Ph2PPr}PDI)Ni was compared. Surprisingly, (^{Ph2PPr}PDI)Co and (^{Ph2PPr}PDI)Mn were found to exhibit higher turnover frequencies, while (^{Ph2PPr}PDI)Fe and (^{Ph2PPr}PDI)Ni were considerably less effective. Further investigation into electronic structure reveals electron count and antiferromagnetically coupled ligand-centered radicals may promote higher activity.

1.2 Introduction

The catalytic hydrosilylation of carbonyl groups represents an efficient, one-step preparation of silyl-protected alcohols. Avoiding the use of stoichiometric amounts of metal hydrides such as $LiAlH_4$ and $NaBH_4$ is appealing to the synthetic community since these reagents are pyrophoric and capable of reducing neighboring functional groups.[1] To date, precious metal catalyzed carbonyl hydrosilylation dominates the field,[2,3,4] but due to growing scarcity and the potential toxicity [5,6] of these metals; base metal catalyzed reactions featuring Mn (4900 min^{-1}),[7] Fe (240 min^{-1}),[8] and Ni (222.5 min^{-1}),[9] have emerged as effective, greener alternatives. While many examples of cobalt mediated alkene and alkyne [10] hydrosilylation have been reported within the last decade, cobalt mediated carbonyl hydrosilylation has remained underdeveloped. In 2012, Gade and workers reported a cobalt alkyl complex, that is active for the asymmetric hydrosilylation of several prochiral alkyl aryl ketones with high yields (up to >99%) and enantioselectivity (91% *ee*) (THF, 2.5 mol % cat., 0 °C, 8 h, $PhSiH_3$).[11] In 2019, Nakazawa and workers developed a bipyridine $CoBr_2$ precatalyst for carbonyl hydrosilylation with low loadings (neat, 0.1 mol % cat., rt, 24 h, 1 mol % $NaEt_3BH$, Ph_2SiH_2).[12] Also in 2019, Moret and workers developed a well-defined cobalt catalyst, κ^3-*P*,*O*,*P*-($^{p\text{-toly}}$)Co, that achieved >99% conversion after 4 h at ambient temperature (neat, 1 mol % cat., $PhSiH_3$).[13] The highest achievable turnover frequency (TOF) of each catalyst was 0.083, 0.604, 0.416 min^{-1}, respectively.

In 2014, our group reported that the bis(imino)pyridine supported Mn catalyst, (^{Ph2PPr}PDI)Mn (Figure 1.1), mediates the hydrosilylation of ketones at room temperature,

displaying TOFs of up to 1280 min^{-1}.[14] Equimolar cyclohexanone and $PhSiH_3$ was added to 0.01 mol % (^{Ph2PPr}PDI)Mn under neat conditions for 5 min, which resulted in >99% conversion. Additionally, equimolar solutions of ethyl acetate and $PhSiH_3$ were added to 1 mol % (^{Ph2PPr}PDI)Mn, which resulted in >99% conversion to a mixture of silyl ethers after 5 h. Inspired by the results, less sterically demanding substrates such as aldehydes and formates were investigated.[15] Addition of an equimolar solution of benzaldehyde and $PhSiH_3$ to 0.01 mol % (^{Ph2PPr}PDI)Mn at 25 °C resulted in >99 % conversion after 2 min. Lastly, an equimolar solution of benzyl formate and $PhSiH_3$ in the presence of 0.02 mol % (^{Ph2PPr}PDI)Mn at 25 °C resulted in >99 % conversion after 15 min. Hydrolysis using 10 % NaOH, followed by extraction afforded good isolated yields of the corresponding alcohols. To date, the TOFs demonstrated for aldehyde hydrosilylation (4900 min^{-1}) and formate dihydrosilylation (330 min^{-1}) are among the highest ever reported.[15]

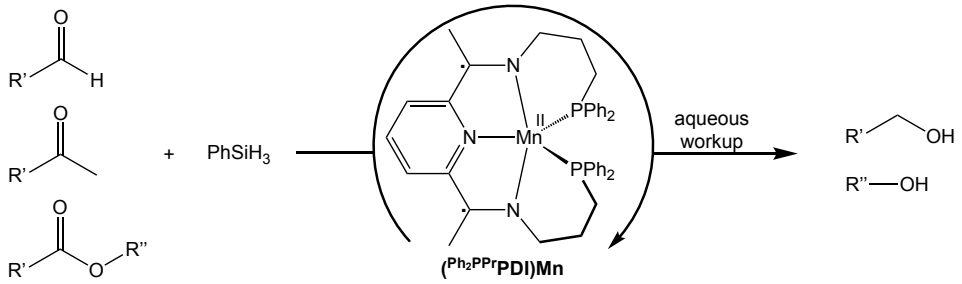

FIGURE 1.1. Carbonyl and carboxylate hydrosilylation catalyzed by (^{Ph2PPr}PDI)Mn

The ability of (^{Ph2PPr}PDI)Mn to catalyze carbonyl hydrosilylation at mild conditions with high activity enticed us to investigate similar iron, cobalt, and nickel ^{Ph2PPr}PDI catalysts for this reaction. Using the same ^{Ph2PPr}PDI ligand, we set out to synthesize and compare the activity of the formally zerovalent Mn (17 e^-), Fe (18 e^-), Co (19 e^-), and Ni (20 e^-) complexes (Figure 1.2). Utilization of this redox-active ligand is critical for developing an understanding of how electronic structure influences catalytic activity. Once

synthesized, these compounds were evaluated for the hydrosilylation of carbonyls at 0.01 mol % loading to investigate if electron count plays a role in catalytic activity. Herein, we discuss the use of ^{Ph2PPr}PDI to evaluate and compare the activity of first row transition metal hydrosilylation catalysts.

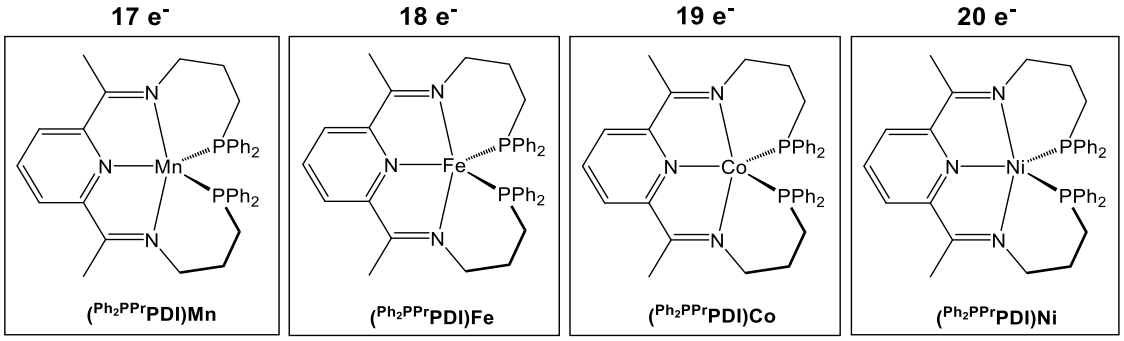

FIGURE 1.2. Targeted metal complexes and their formal electron count.

1.3 Results and Discussion

This study began with the preparation of (^{Ph2PPr}PDI)Mn, (**1**) via Na/Hg reduction of (^{Ph2PPr}PDI)$MnCl_2$ in the presence of 1,3,5,7-cyclooctatetraene (COT).[14] This complex was previously found to be paramagnetic (2.2 μ_B, 23 °C) and is known to exhibit a ^{1}H NMR spectrum that features 10 broadened resonances that are shifted over a 200 ppm range. Single crystal X-ray diffraction revealed a 5-coordinate distorted trigonal bipyramidal geometry around the metal center that features a PDI chelate possessing significantly elongated N(1)−C(2) and N(3)−C(8) distances of 1.354(3) and 1.355(3) Å, along with contracted C(2)−C(3) and C(7)−C(8) distances of 1.416(4) and 1.414(3) Å, respectively. Previously reported ($^{2,6\text{-iPr2Ph}}$PDI)Mn(THF)$_2$ [16] was found to possess similar bond lengths around a low-spin Mn(II) center that is supported by a singlet PDI dianion. The electron paramagnetic resonance (EPR) spectrum of **1** is consistent with a low-spin Mn(II) center. With **1** in hand, ketone hydrosilylation was evaluated using 0.01 mol % at 25 °C. Notably,

cyclohexanone was completely converted to the corresponding silyl ether using $PhSiH_3$ in 5 min, allowing for a TOF of 1280 min^{-1}.[14]

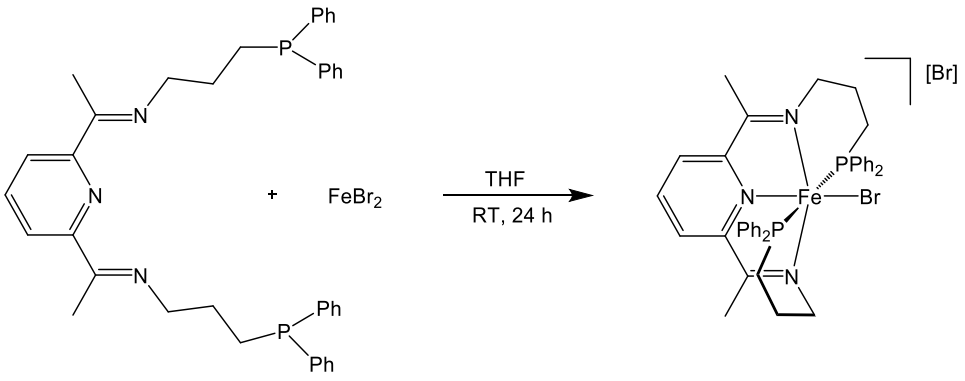

FIGURE 1.3. Synthesis of [(^{Ph2PPr}PDI)FeBr][Br] (**2**).

Knowing that (^{Ph2PPr}PDI)Mn is highly-active for carbonyl hydrosilylation, we sought to prepare the Fe, Co, and Ni analogs. The synthesis of [(^{Ph2PPr}PDI)FeBr][Br] (**2**) (Figure 1.3) began with the addition of ^{Ph2PPr}PDI[17] to $FeBr_2$ in THF solution. Multinuclear NMR spectroscopy suggested that the resulting purple compound is diamagnetic. The ^{1}H NMR spectrum (Figure 1.4) displays a single backbone methyl peak at 1.31 ppm, indicating C_2-symmetry. The ^{31}P NMR spectrum of this complex features a single resonance for both phosphine atoms at 31.46 ppm (Figure 1.5).

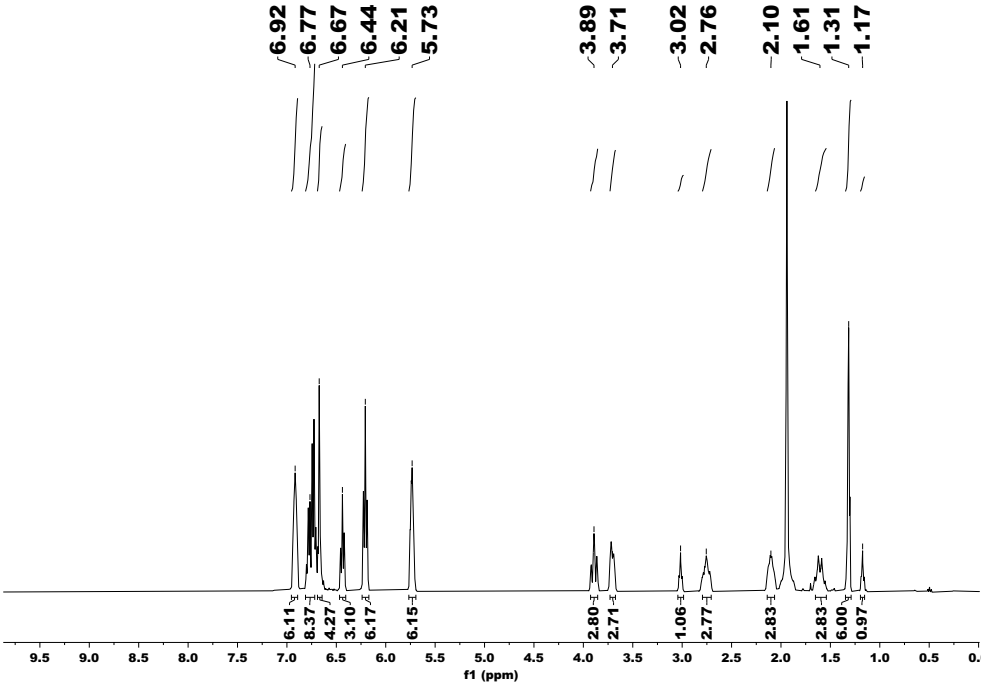

FIGURE 1.4. ^{1}H NMR spectrum of **2** in acetone-d_6 at 25 °C.

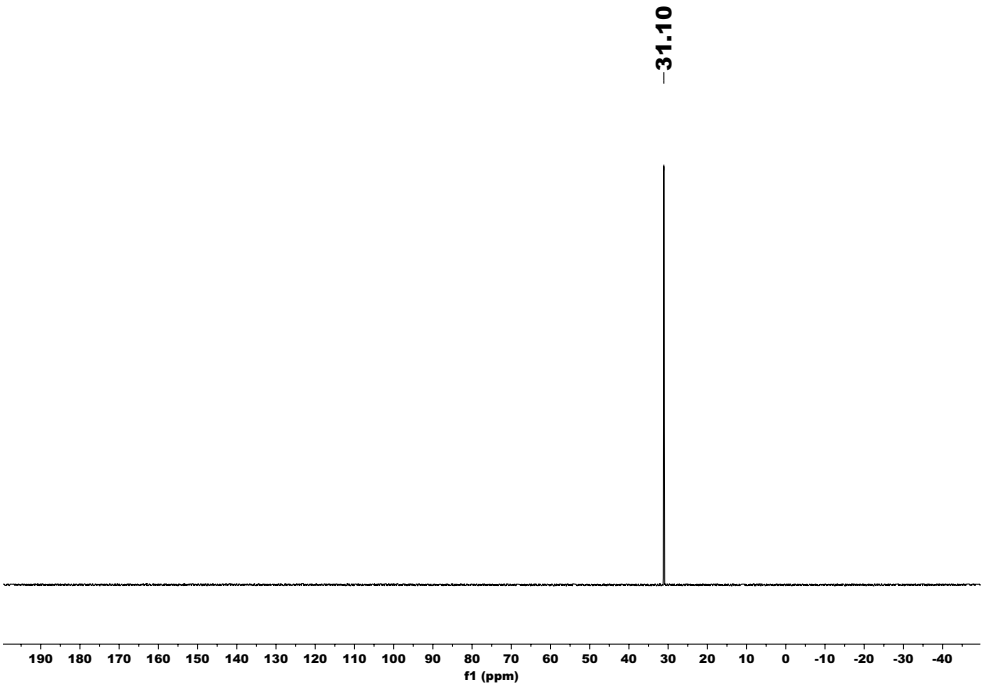

FIGURE 1.5. ^{31}P NMR spectrum of **2** in acetone-d_6 at 25 °C.

Reduction of **2** with excess Na/Hg followed by work up to remove NaBr yielded a greenish-brown compound identified as (^{Ph2PPr}PDI)Fe (**3**) (Figure 1.6) after 48 h. Similar to compound **2**, the ^{31}P spectrum of **3** shows a single peak at 69.81 ppm, indicating that both phosphine arms are bound to the iron center. Additionally, the C_2-symmetry of this compound is reflected in its ^{1}H NMR spectrum, which showed a single resonance for both backbone methyl groups. Single crystals suitable for X-ray diffraction were obtained by Chandrani Ghosh and analysis revealed (κ^5-*N*,*N*,*N*,*N*,*P*,*P*-^{Ph2PPr}PDI)Fe (Figure 1.7), which was present as two unique molecules in the asymmetric unit. Each molecule has a pseudo trigonal bipyramidal geometry around iron with N(1)–Fe(1)–N(3) angles of 159.22(13) and 160.28(11)° and P(1)–M(1)–P(2) angles of 102.23(4)° and 103.95(3)° for molecules 'A' and 'B', respectively (Table 1.1). Additionally, the Fe(1)-N(2) lengths were found to be 1.837(3) and 1.833(2) Å, which are considerably shorter than the Mn(1)-N(2) length of 1.887(2) Å for **1**.[14]

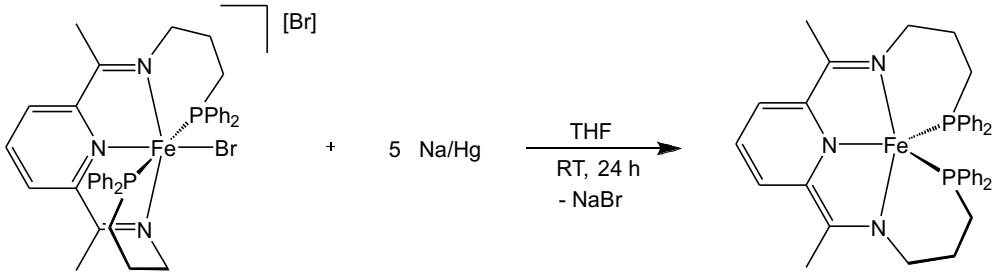

FIGURE 1.6. Synthesis of (^{Ph2PPr}PDI)Fe (**3**).

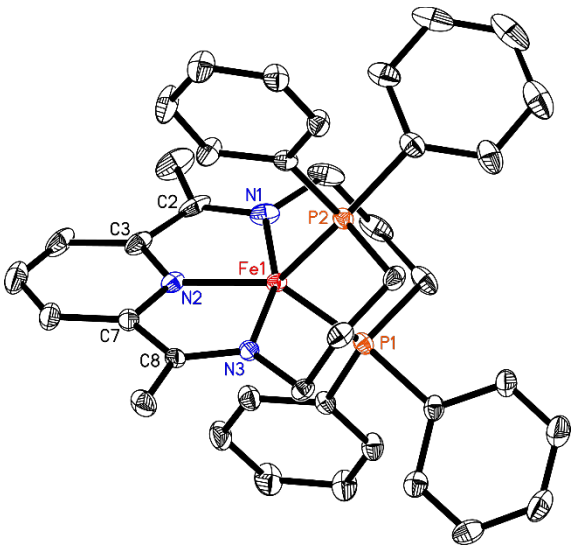

FIGURE 1.7. Molecular structure of **3** at 30% probability ellipsoids. Hydrogen atoms omitted for clarity.

TABLE 1.1. Selected bond lengths (Å) and angles (°) for **3**.

Fe(1)–N(1)	1.935(3)/1.930(3)	N(1)–C(2)	1.337(5)/1.338(4)
Fe(1)–N(2)	1.837(3)/1.833(2)	N(3)–C(8)	1.339(4)/1.341(4)
Fe(1)–N(3)	1.924(3)/1.935(3)	C(2)–C(3)	1.416(6)/1.422(4)
Fe(1)–P(1)	2.1795(10)/2.1843(9)	C(7)–C(8)	1.410(5)/1.418(4)
Fe(1)–P(2)	2.1735(10)/2.1768(9)	N(1)-Fe(1)-N(3)	159.22(13)/160.28(11)

Next, [(^{Ph2PPr}PDI)Co][Cl] (**4**) (Figure 1.8) was prepared following the addition of ^{Ph2PPr}PDI to $(Ph_3P)_3CoCl$ in THF solution. After stirring for 24 h, **4** was obtained as an insoluble, forest green compound. Multinuclear NMR spectroscopy suggested that this product is diamagnetic. The ^{1}H NMR spectrum of **4** indicates C_2-symmetry and features a single resonance for the backbone methyl groups (Figure 1.9). Additionally, the ^{31}P NMR spectrum of this complex featured a single resonance for both phosphine arms at 43.00 ppm (Figure 1.10). Recrystallization of **4** from chloroform at –35 °C afforded single crystals suitable for X-ray diffraction analysis, which confirmed a distorted trigonal bipyramidal coordination environment about Co with an N(1)–Co(1)–N(3) angle of 161.22° (Figure 1.11). Although the data is not suitable for publication, the N(1)-C(3) length of 1.291 Å suggests that the chelate is not reduced.

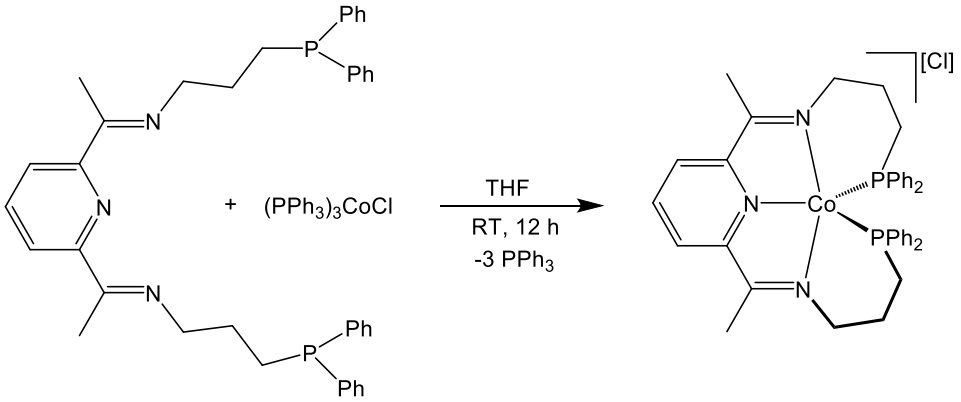

FIGURE 1.8. Synthesis of [(^{Ph2PPr}PDI)Co][Cl] (**4**).

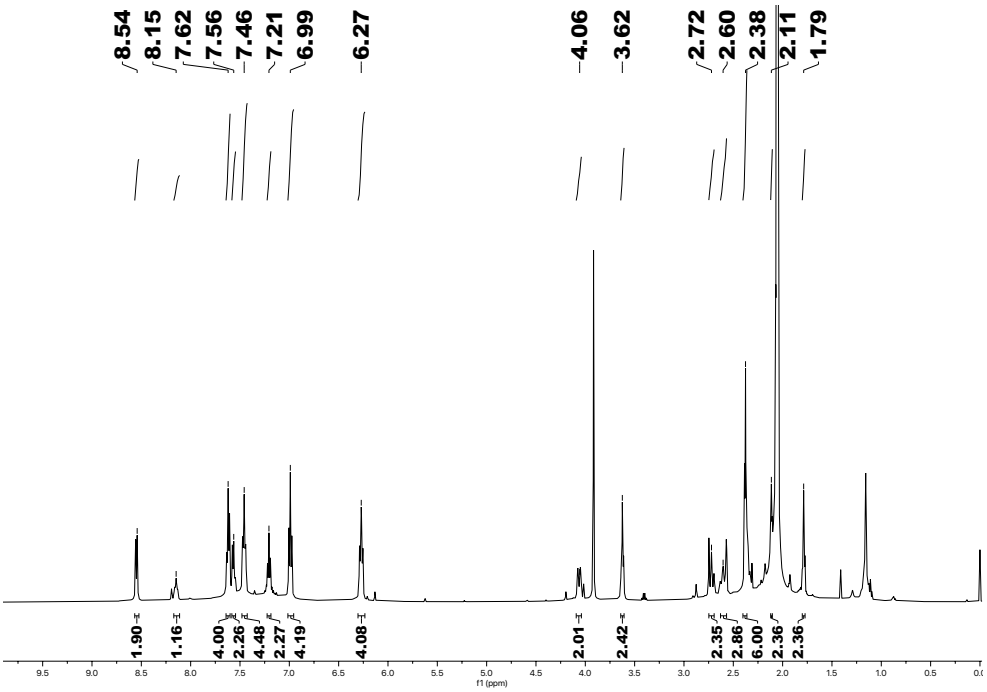

FIGURE 1.9. ^{1}H NMR spectrum of **4** in acetone-d_6 at 25 °C.

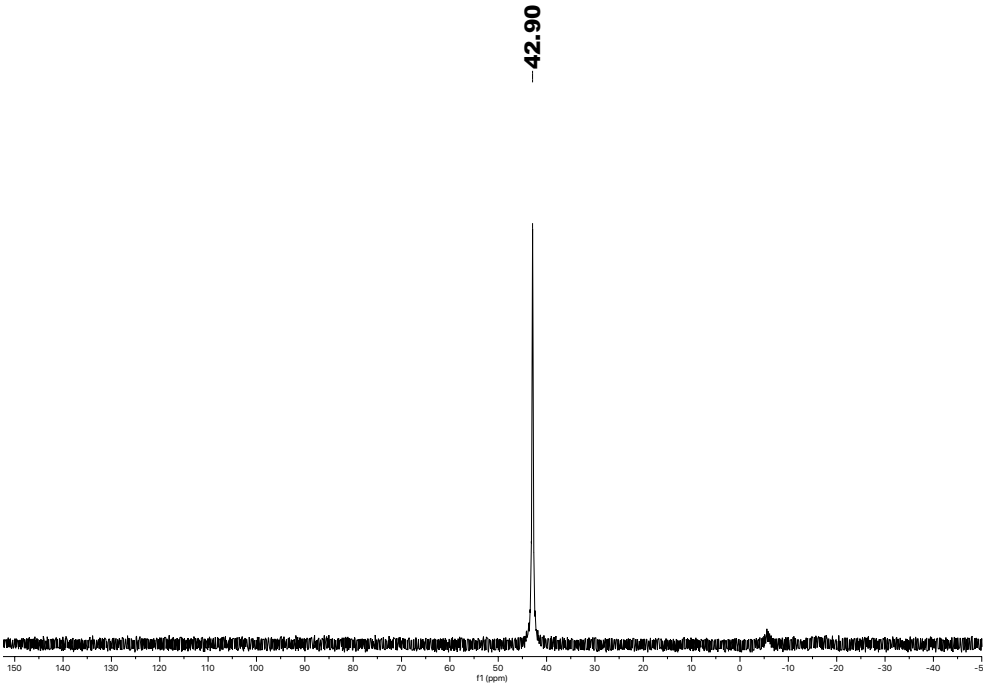

FIGURE 1.10. ^{31}P NMR spectrum of **4** in acetone-d_6 at 25 °C.

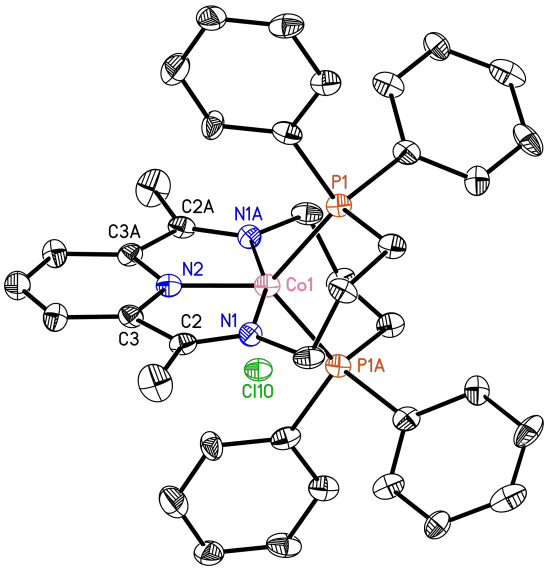

FIGURE 1.11. Molecular structure of **4** at 30% probability ellipsoids. Hydrogen atoms omitted for clarity.

TABLE 1.2. Selected bond lengths (Å) and angles (°) for **4**.

Co(1)–P(1)	2.2054	N(1)–C(2)	1.2913
Co(1)–N(1)	1.9266	C(2)–C(3)	1.4434
Co(1)–N(2)	1.9266	N(1)-Co(1)-N(1)	161.22

Reduction of **4** with excess Na/Hg for 48 h and workup to remove NaCl afforded the formally zerovalent complex, (^{Ph2PPr}PDI)Co (**5**) (Figure 1.12). The ^{1}H NMR spectrum of this complex features 12 broadened resonances that are shifted over a 100 ppm range (Figure 1.13). The complex was found to have an effective magnetic moment of 1.67 μ_B at 23 °C (S_{Co} = ½), which is consistent with one unpaired electron. Preliminary DFT calculations have suggested **5** to be a high-spin Co(I) center that is antiferromagnetically coupled to an electron on the PDI chelate, resulting in one unpaired electron located on the metal.

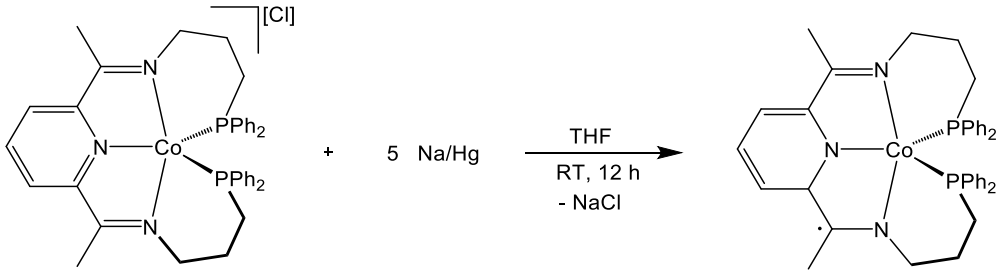

FIGURE 1.12. Synthesis of (^{Ph2PPr}PDI)Co (**5**).

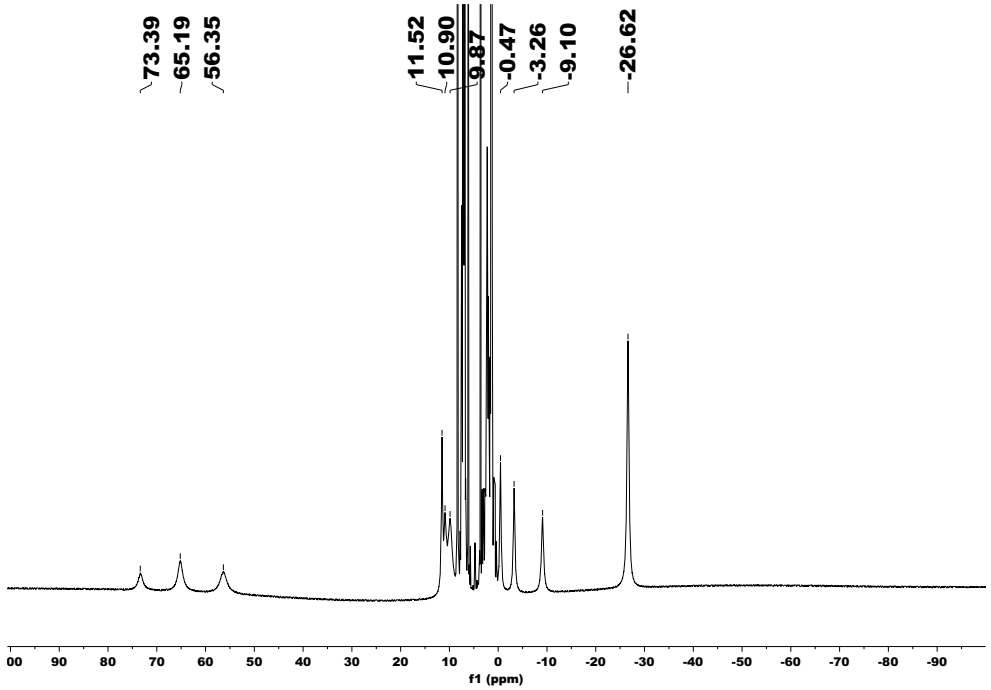

FIGURE 1.13. ^{1}H NMR spectrum of **5** in benzene-d_6 at 25 °C.

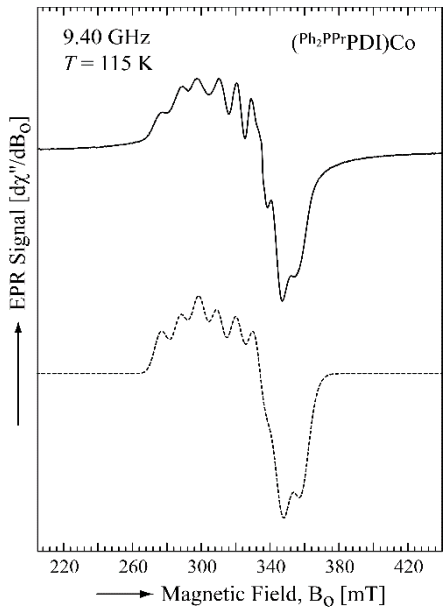

FIGURE 1.14. Experimental (solid line) and simulated (dashed line) X-band EPR spectra of **5** at 115 K.

To obtain additional electronic information, the X-band (9.40 GHz) electron paramagnetic resonance (EPR) spectrum of **5** was recorded in a toluene glass at 115 K by Hagit Ben-Daat and Marco Flores. The observed spectral features are consistent with the presence of a S = ½ species, i.e., the signal was centered around the magnetic field value corresponding to g = 2.0 (Figure 1.14). Additionally, hyperfine coupling (hfc) was observed between the magnetic moment of the unpaired electron and the magnetic moment of the ^{59}Co (I = 7/2) nucleus, which is evident in the multiline spectrum in Figure 1.14. To obtain the EPR parameters, the respective spin Hamiltonian was fit to the data (Figure 1.14, dotted line). The EPR spectrum of **5** was well-fit (σ = 2.8 %, see Section 1.8) considering one unpaired electron on a ^{59}Co center (S_{Co} = ½, I = 7/2) with anisotropic g values (g_x = 2.120, g_y = 2.105, g_z = 1.969) and large anisotropic hyperfine couplings (| A_x | = 334.0, | A_y | = 154.6, | A_z | = 1.6 MHz) (see Table 1.4). These properties are similar to those previously reported for the ^{55}Mn center (S_{Mn} = ½, I = 5/2) in compound **1**,[14] suggesting that the

coordination environment about Co in **5** is similar to the crystallographically determined coordination environment about Mn in **1**.

TABLE 1.3. Parameters used to fit the EPR spectra of **5** and **6** at X-band (9.4 GHz) and low temperature.

Parameter[a]	**5** (Co) (T = 115 K)	**6** (Ni)[b] (T = 112 K)
g_x	2.120	2.199
g_y	2.105	2.125
g_z	1.969	2.023
$\lvert A_x \rvert$ (MHz)	334.0	–[c]
$\lvert A_y \rvert$ (MHz)	154.6	–
$\lvert A_z \rvert$ (MHz)	1.6	–
ΔB_x (MHz)	257.9	296.6
ΔB_y (MHz)	405.9	279.9
ΔB_z (MHz)	520.4	270.8

[a]The fitting parameters were the principal components of $\boldsymbol{g}$ (i.e. g_x, g_y, and g_z), the principal components of the hfc tensor $\boldsymbol{A}$ (i.e. A_x, A_y, and A_z), and the peak-to-peak line widths (ΔB_x, ΔB_y, and ΔB_z). [b]The EPR spectrum of this compound showed the signals of two uncoupled S = 1/2 spins, one corresponding to Ni(I) (for parameters see at the table) and another one corresponding to a ligand radical ($PDI^{\bullet-}$) with the following parameters: g_x = 2.012, g_y = 2.005, and g_z = 1.991; ΔB_x = 61.8 MHz, ΔB_y = 59.4 MHz, and ΔB_z = 105.4 MHz. [c]Ni has nuclear spin (I = 3/2) but its natural abundance is only 1.14%, so the respective hfc interaction cannot be resolved in the EPR spectrum of Ni(I).[18]

Finally, (^{Ph2PPr}PDI)Ni was prepared following the addition of $Ni(COD)_2$ to ^{Ph2PPr}PDI in toluene solution (Figure 1.15). After stirring for 24 h, an olive-green compound (**6**) was collected after workup. Analysis by ^{1}H NMR spectroscopy revealed the complete disappearance of $Ni(COD)_2$ and the formation of a new paramagnetic complex that featured 8 broadened resonances shifted over a 29 ppm range (Figure 1.16). The complex was found to have an effective magnetic moment of 1.23 μ_B at 23 °C. Single crystals

suitable for X-ray diffraction were obtained by Tyler Porter and analysis revealed the complex to be (κ^4-*N*,*N*,*N*,*P*-^{Ph2PPr}PDI)Ni (Figure 1.17). The geometry about the nickel center is best described as distorted square planar with N(3)-Ni(1)-N(1) and P(1)-Ni(1)-N(2) angles of 150.8° and 151.8°, respectively. Additionally, the PDI chelate features significantly elongated N(1)-C(2) and N(3)-C(8) distances of 1.337(7) and 1.340(7) Å, along with contracted C(2)-C(3) and C(8)-C(7) distances of 1.427(8) and 1.429(9) Å, respectively (Table 1.4). These bond distances suggest that **6** contains a PDI monoradical anion. The small magnetic moment observed suggests the possibility of weak electronic coupling between the Ni and PDI-based electrons.

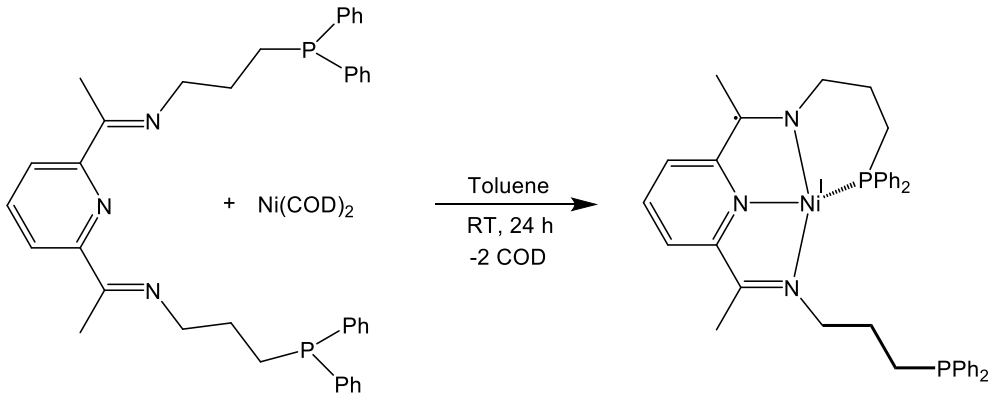

FIGURE 1.15. Synthesis of (^{Ph2PPr}PDI)Ni (**6**).

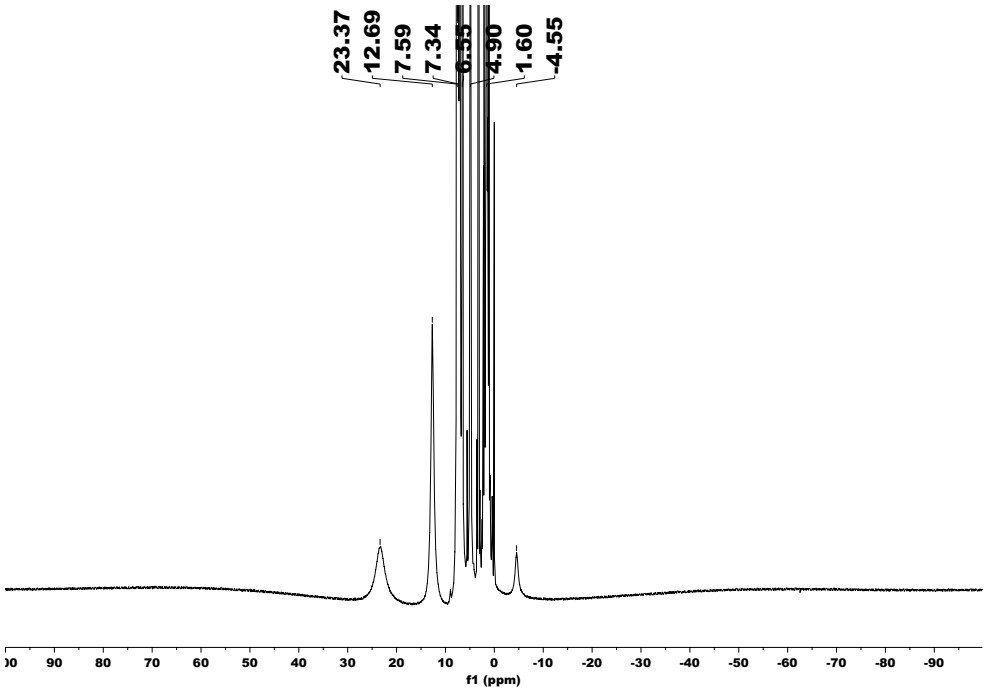

FIGURE 1.16. ^{1}H NMR spectrum of **6** in benzene-d_6 at 25 °C.

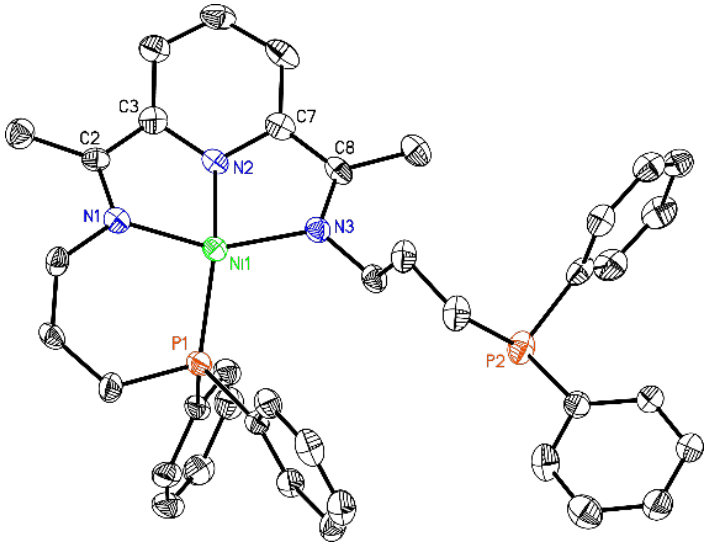

FIGURE 1.17. Molecular structure of **6** at 30% probability ellipsoids. Hydrogen atoms omitted for clarity.

TABLE 1.4. Selected bond lengths (Å) and angles (°) for **6**.

Ni(1)–N(1)	1.937(5)	N(1)–C(2)	1.340(7)
Ni(1)–N(2)	1.872(4)	N(3)–C(8)	1.337(7)
Ni(1)–N(3)	1.947(5)	C(2)–C(3)	1.427(8)
Ni(1)–P(1)	2.1574(17)	C(7)–C(8)	1.429(9)
Ni(1)–P(2)	-	N(1)-Ni(1)-N(3)	150.8(2)

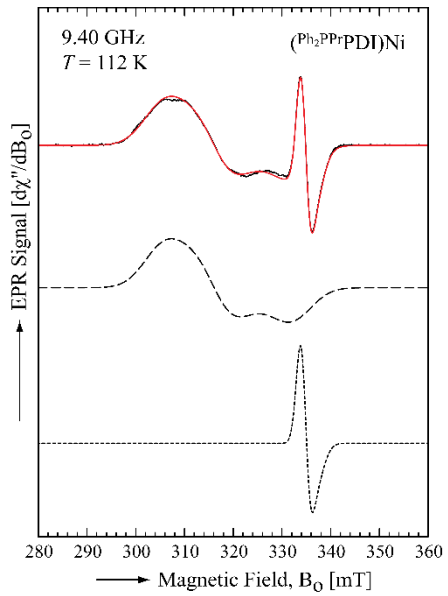

FIGURE 1.18. Experimental (solid black line) and simulated (solid red line) X-band EPR spectra of **6** at 112 K. Simulation of the spectral components corresponding to a Ni(I) center (dashed line) and a PDI radical anion (dotted line) are also shown. The sum of the spectral components results in the simulated spectrum (solid red line).

To obtain supporting evidence for this electronic structure determination, the X-band (9.40 GHz) electron paramagnetic resonance (EPR) spectrum of **6** was recorded in a toluene glass at 112 K (Figure 1.16). The observed spectrum is an overlap of two $S = ½$ signals, a narrow isotropic-like signal located at the magnetic field value corresponding to $g = 2.0$ and a broad signal showing significant rhombic g anisotropy. To obtain the EPR parameters, the respective spin Hamiltonian was fit to the data (Figure 1.18, red line) while

assuming that the broad signal belongs to the unpaired electron of a Ni(I) center (S_{Ni} = ½) (Figure 1.18, dashed line) and the narrow signal belongs to an unpaired electron located within the PDI ligand ($PDI^{\bullet-}$) (Figure 1.18, dotted line). The spectral features observed for **6** were well-fit (σ = 0.6 %, see Section 1.8) when treating this complex as carrying a Ni(I) center and a PDI radical anion that are not magnetically coupled (see Table 1.4). Preliminary DFT calculations have suggested that the singly occupied Ni-based and PDI-based orbitals are spatially non-orthogonal, which suggests that the unpaired electrons are ferromagnetically uncoupled.

1.4 Evaluation of Carbonyl Hydrosilylation Activity

With **1, 3**, **5**, and **6** synthesized, their ability to hydrosilylate benzaldehyde at 25 °C was evaluated. Compound **1** was previously shown to achieve >99% conversion (TOF = 4900 min^{-1}) after 2 min at 25 °C.[14] To begin, an equimolar solution of benzaldehyde and $PhSiH_3$ was added to a scintillation vial containing 0.01 mol % of **3**, **5**, and **6** as shown in Table 1.5. When **3** was employed, no immediate bubbling was noticed nor was any heat evolved from the reaction flask and quenching with I_2 after 2 min resulted in 11% conversion (TOF = 550 min^{-1}). However, when the reaction was performed and then exposed to air, the solution became extremely hot and bubbled profusely, resulting in >99% conversion (TOF = 3330 min^{-1}) after 1 min of air exposure and dissolving in wet benzene-d_6. Repeating the experiment and quenching with water after 2 min resulted in 78% conversion (TOF = 3900 min^{-1}) which resulted from air exposure prior to catalyst death. When **5** was employed, immediate bubbling and extreme heat evolved from the reaction flask, resulting in >98% (4900 min^{-1}) after 2 min. When **6** was employed, no bubbling or heat was observed and 40% conversion (TOF = 2000 min^{-1}) was observed after 2 min.

TABLE 1.5. Benzaldehyde hydrosilylation at 0.01 mol% catalyst loading.

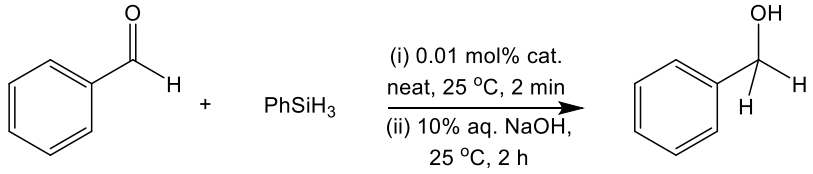

Entry	Catalyst	% Conversion[a]	Isolated Yield%	TOF (min^{-1})
1[15]	**1**	>99%	92%	4950
2	**3**	11%	-	550
3	**5**	>98%	83%	4900
4	**6**	40%	-	2000

[a]Percent conversion determined by ^{1}H NMR spectroscopy (integration of residual benzaldehyde vs. silyl ether product).

Similar conditions were employed for the hydrosilylation of acetophenone, which is more difficult to reduce than benzaldehyde, for steric reasons. An equimolar solution containing acetophenone and $PhSiH_3$ was added to 0.01 mol % **1**, **3**, **5**, and **6** (Table 1.6). When catalyst **1** was used, immediate bubbling and extreme heat was observed which resulted in >99% conversion (TOF = 4950 min^{-1}) after 2 min. When **3** was employed, no bubbling or heat was observed from the reaction flask and quenching with I_2 after 2 min resulted in 5% conversion (TOF = 250 min^{-1}). However, when this reaction was quenched by exposing to air, the solution became moderately hot affording 52% conversion (TOF = 1733 min^{-1}) after 1 min of air exposure. When **5** was employed, immediate bubbling and extreme heat evolved from the reaction flask, which resulted in 82% conversion (4100 min^{-1}) after 2 min. When **6** was employed, no bubbling or heat was observed and <1% conversion was observed after 2 min.

TABLE 1.6. Acetophenone hydrosilylation at 0.01 mol% catalyst loading.

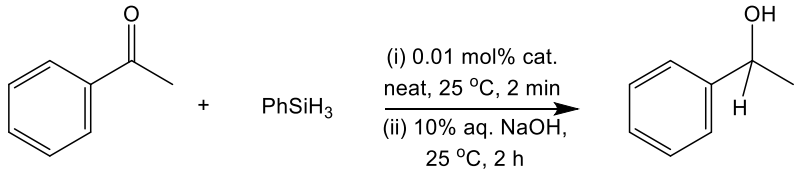

Entry	Catalyst	% Conversion[a]	Isolated Yield%	TOF (min^{-1})
1	**1**	>99%	92%	4950
2	**3**	5%	-	250
3	**5**	82%	-	4100
4	**6**	<1	-	<50

[a]Percent conversion determined by ^{1}H NMR spectroscopy (integration of residual acetophenone vs. silyl ether product).

1.5 Origins of Activity

By investigating late metal ^{Ph2PPr}PDI complexes for carbonyl hydrosilylation, trends in electronic structure appear to be responsible for differences in observed catalytic activity. In the case of **1**, this complex was found to possess a low-spin Mn(II) center (μ_{eff} = 2.2 μ_B, 23 °C) that is chelated by a PDI dianion. EPR spectroscopy revealed an unpaired electron on the metal. Similar to **1**, **5** was found to have an effective magnetic moment of 1.67 μ_B at 23 °C. EPR spectroscopy of **5** revealed an unpaired electron on the metal. While efforts to obtain single crystals of **5** for X-ray diffraction remain unfruitful, the EPR parameters of **5** suggest that the coordination environment around **5** is similar to that of **1**.[14] Given that **1** engages in Si-H oxidative addition following phosphine dissociation to generate an active M-H species that participates in a modified Ojima pathway, it is reasonable to suggest that the mechanism of **5**-catalyzed carbonyl hydrosilylation also relies on M-P bond dissociation.

In contrast, **3** and **6** exhibit low carbonyl hydrosilylation activity. One similarity between the complexes is an even formal electron count. In the case of **3**, single crystal X-ray diffraction revealed a singlet PDI dianion that supports an Fe(II) center. However, single crystal X-ray diffraction analysis of **6** revealed a PDI chelate that is reduced by one electron that does not couple to the Ni(I) center. Although, both **3** and **6** feature a reduced PDI chelate; M-P bond dissociation may not occur as easily. Looking at formal electron counts, we suspect that even counts result in lower activity due to stronger M-P bonding. Interestingly, antiferromagnetic coupling of the metal to a PDI-ligand radical could also be responsible for higher hydrosilylation activity. Although, **3** and **6** have a reduced PDI chelate, antiferromagnetic coupling is not observed, with **3** featuring a singlet PDI dianion and **6** featuring an uncoupled anionic chelate. In contrast, **1** features a triplet PDI dianion that is antiferromagnetically coupled to the metal. Because preliminary DFT studies indicate that **5** features a singly reduced chelate that is antiferromagnetically coupled to the metal, this feature may be important for catalytic activity.

1.6 Substrate Scope

Encouraged after finding that cobalt mediated ketone hydrosilylation occurs at 0.01 mol % loading, the scope of this reaction was evaluated at 0.1 mol % of **5** (Table 1.7). An equimolar quantity of $PhSiH_3$ and acetophenone was added to 0.1 mol % of **5** under neat conditions at 25 °C. After 5 min, the reaction was exposed to air to deactivate the catalyst and NMR spectroscopic analysis revealed complete acetophenone hydrosilylation (TOF = 195 min^{-1}) (Table 1.7, 1a). Treatment with 10% aq. NaOH allowed for the isolation of α-methylbenzyl alcohol (92%, Table 1.7, 1a) following extraction and solvent evaporation. Methoxy-substitution (entry 1b) was found to hinder conversion while fluoro-substitution

(entry 1c) allowed for complete conversion after 10 min. A preliminary screening of functional group tolerance is demonstrated in entries 1b-1f where primary amines and hydroxy groups were found to undergo dehydrocoupling with silanes to form the silyl amine and silyl ether, respectively. The nitrile functionality of 1f was tolerated by **5**, but the reaction required 9 d to reach full conversion, presumably due to nitrile coordination.

TABLE 1.7 Ketone hydrosilylation using (^{Ph2PPr}PDI)Co (**5**).

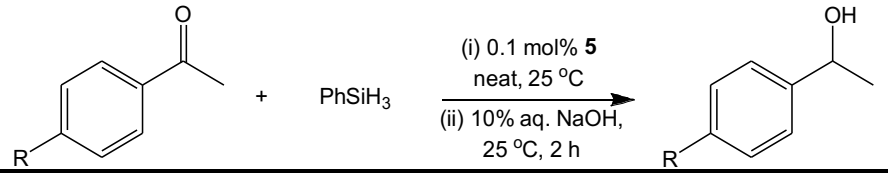

Substrate	Time	% Conv.[a]	Isolated Yield%
1a, R = H	5 min	>99%	92%
1b, R = OMe	2 h	>99%	75%
1c, R = F	10 min	>99%	87%
1d[b], R = NH_2	12.5 h	>99%	72%
1e[c], R = OH	16 h	>99%	-
1f[c], R = CN	9 d	>99%	-

[a]Percent conversion determined by ^{1}H NMR spectroscopy (integration of residual ketones vs. silyl ether products). [b]3 equiv. $PhSiH_3$ was used. [c]2 equiv. $PhSiH_3$ was used.

1.7 Conclusion

Iron, cobalt, and nickel ^{Ph2PPr}PDI complexes have been prepared and characterized using single crystal X-ray diffraction and spectroscopic techniques. By extending this redox-capable ligand framework across the aforementioned metals, electronic and structural trends were evaluated. The (^{Ph2PPr}PDI)Fe complex was found to have an Fe(II) metal center and trigonal bipyramidal geometry. The (^{Ph2PPr}PDI)Co complex was found to possess a Co(I) center due to one electron reduction of the ligand from the metal as found from preliminary DFT studies. In contrast, (^{Ph2PPr}PDI)Ni was found to possess a pseudo

tetrahedral geometry around a Ni(I) core. With the compounds in hand, evaluation of carbonyl hydrosilylation was performed. Interestingly, (^{Ph2PPr}PDI)Co was found to exhibit aldehyde and ketone hydrosilylation TOFs of 4,900 min^{-1} and 4,100 min^{-1}, respectively, making it the most active cobalt catalyst reported to date. Oddly, (^{Ph2PPr}PDI)Fe and (^{Ph2PPr}PDI)Ni were found to exhibit considerably lower TOFs than the Mn and Co analogs. Features present in (^{Ph2PPr}PDI)Mn and (^{Ph2PPr}PDI)Co include an odd electron count and metal-ligand antiferromagnetic coupling. Although, (^{Ph2PPr}PDI)Ni was found to feature a PDI radical anion, antiferromagnetic coupling was not present.

1.8 Experimental

General considerations: All reactions were performed inside an MBraun glovebox under an atmosphere of purified nitrogen. Toluene, tetrahydrofuran, pentane, and diethyl ether were purchased from Sigma-Aldrich, purified using a Pure Process Technology solvent system, and stored in the glovebox over activated 4 Å molecular sieves and sodium before use. Benzene-d_6, acetone-d_6, and chloroform-*d* were purchased from Oakwood Chemicals and dried over 4 Å molecular sieves. 2,6-Diacetylpyridine was obtained from Oakwood Chemicals. Benzaldehyde and acetophenone were purchased from Sigma-Aldrich, while cobalt dichloride was obtained from Strem. ^{Ph2PPr}PDI was synthesized according to literature procedures.[17] Celite was purchased from Acros. Solution ^{1}H NMR spectra were recorded at room temperature on a Varian 400-MR (400 MHz), Varian 500-MR (500 MHz), Bruker Ascend 400 MHz, or Bruker Ascend 500 MHz NMR spectrometer. All ^{1}H NMR and ^{13}C NMR chemical shifts are reported in parts per million relative to $Si(CH_3)_4$ using internal $Si(CH_3)_4$ or ^{1}H (residual) and ^{13}C chemical shifts of the solvent as secondary standards. Elemental analyses were performed at Robertson Microlit Laboratories, Inc.

(Ledgewood, NJ). Solution-state magnetic susceptibility was determined via the Evans method on the Varian 400-MR (400 MHz) NMR spectrometer.

Electron Paramagnetic Resonance Spectroscopy:

Instrumentation. Studies were performed at the EPR Laboratory, part of the Chemical and Environmental Characterization Core Facilities at Arizona State University. Continuous wave (CW) EPR spectra were recorded at 115 K for **5** and 112 K for **6** using a Bruker ELEXSYS E580 CW X-band spectrometer (Bruker, Rheinstetten, Germany) equipped with a liquid nitrogen temperature control system (ER 4131VT). The magnetic field modulation frequency was 100 kHz with a field modulation amplitude of 1 mT peak-to-peak. The microwave power was 4 mW for **5** and 1 mW for **6**, the microwave frequency was 9.40 GHz and the sweep time was 168 seconds for **5** and 84 seconds for **6**.

Spin Hamiltonian. The EPR spectrum of **5** was interpreted using a $S = ½$ spin Hamiltonian, H, containing the electron Zeeman interaction with the applied magnetic field $\mathbf{B_0}$, and the hyperfine coupling (hfc) interaction with the ^{59}Co (I = 7/2) nucleus:[19]

$$H = b_e\, \mathbf{S} \,.\, \boldsymbol{g} \,.\, \mathbf{B_0} + h\, \mathbf{S} \,.\, \boldsymbol{A} \,.\, \mathbf{I} \qquad (1)$$

where **S** is the electron spin operator, **I** is the nuclear spin operator of ^{59}Co, $\boldsymbol{A}$ is the hfc tensor in frequency units, $\boldsymbol{g}$ is the electronic g-tensor, b_e is the electron magneton, and h is Planck's constant.

The EPR spectrum of **6** was analyzed considering that the molecule contains two $S = ½$ spins. One corresponds to the unpaired electron of a Ni(I) center (denoted by S_A) and the other belongs to the unpaired electron at the PDI radical anion (denoted by S_B). They interact with the applied magnetic field $\mathbf{B_0}$ (Zeeman interaction) but not with each other. The spin Hamiltonian, H', of this system is:

$$H' = b_e \mathbf{S_A} \cdot \boldsymbol{g}_{\mathbf{Ni}} \cdot \mathbf{B_0} + b_e \mathbf{S_B} \cdot \boldsymbol{g}_{\mathbf{PDI}} \cdot \mathbf{B_0} \qquad (2)$$

where $\mathbf{S_A}$ and $\mathbf{S_B}$ are the corresponding electron spin operators, $\boldsymbol{g}_{\mathbf{Ni}}$ and $\boldsymbol{g}_{\mathbf{PDI}}$ are the electronic *g*-tensors for the Ni(I) center and the PDI radical anion, respectively.

Fitting of EPR spectra. To quantitatively compare experimental and simulated spectra, we divided the spectra into N intervals, i.e. we treated the spectrum as an N-dimensional vector **R**. Each component R_j has the amplitude of the EPR signal at a magnetic field B_j, with j varying from 1 to N. The amplitudes of the experimental and simulated spectra were normalized so that the span between the maximum and minimum values of R_j is 1. We compared the calculated amplitudes R_j^{calc} of the signal with the observed values R_j defining a root-mean-square deviation s by:

$$s(p_1, p_2,\ldots, p_n) = [\ (R_j^{calc}(p_1, p_2, \ldots, p_n) - R_j^{exp})^2/N]^{1/2} \qquad (3)$$

where the sums are over the N values of j, and p's are the fitting parameters that produced the calculated spectrum. For our simulations, N was set equal to 2048 for **5** and 1024 for **6**. The EPR spectrum was simulated using EasySpin (v 5.2.25), a computational package developed by Stoll and Schweiger[20] and based on Matlab (The MathWorks, Natick, MA, USA). EasySpin calculates EPR resonance fields using the energies of the states of the spin system obtained by direct diagonalization of the spin Hamiltonian (see Eqs. 1 and 2). The EPR fitting procedure used a Monte Carlo type iteration to minimize the root-mean-square deviation, σ (see Eq. 3) between measured and simulated spectra. We searched for the optimum values of the following parameters: the principal components of $\boldsymbol{g}$ (i.e. g_x, g_y, and g_z), the principal components of the hfc tensor $\boldsymbol{A}$ (i.e. A_x, A_y, and A_z) and the peak-to-peak linewidths (ΔB_x, ΔB_y, and ΔB_z).

Preparation of [(^{Ph2PPr}PDI)FeBr][Br] (2):

Under a nitrogen atmosphere, a 20 mL scintillation vial was charged with 0.123 g (0.572 mmol) of $FeBr_2$ in approximately 5 mL of THF and stirred for 10 min until $FeBr_2$ was almost dissolved. To this, a solution of 0.351 g (0.572 mmol) ^{Ph2PPr}PDI in approximately 5 mL THF was added and an immediate color change from light brown to purple was observed. The reaction was allowed to stir for 24 h at room temperature and then filtered. An insoluble purple solid compound was collected from the top of the frit. The solid was washed with ether (3 x 5 mL) followed by pentane (3 x 5 mL) to obtain 0.398 g of [(^{Ph2PPr}PDI)FeBr][Br] (yield = 84%). Anal. Cald. for $C_{39}H_{41}N_3FeP_2Br_2$: Cald. C, 56.48%; H, 4.98%; N, 5.07%. Found: C, 55.54%; H, 4.69%; N, 4.89%. ^{1}H NMR (400 MHz, acetone-d_6): 6.90 (d, J = 16.6 Hz, 4H, phenyl), 6.82 (m, 2H, *phenyl*), 6.62 – 6.59 (m, 6H, *phenyl*), 6.34 (t, J = 7.3 Hz, 2H, *phenyl*), 6.14 (t, J = 7.6 Hz, 4H, *phenyl*), 5.78 – 5.71 (m, 4H, *phenyl*) 3.93 (t, J = 12.1 Hz, 2H, -CH_2), 3.75 (d, J = 12.2 Hz, 2H, -CH_2), 2.78 – 2.66 (m, 2H, -CH_2), 2.05 (m, 2H, -CH_2), 2.01 (s, 6H, -CH_3), 1.89 (dd, J = 28.3, 15.0 Hz, 2H, -CH_2), 1.74 – 1.59 (m, 2H, -CH_2). ^{31}P NMR (202.47 MHz, acetone-d_6, 25 °C): 31.10 (s, Fe-*P*).

Preparation of (^{Ph2PPr}PDI)Fe (3):

Under a nitrogen atmosphere, a 20 mL scintillation vial was charged with 3.81 g of mercury (19.06 mmol) followed by freshly cut sodium (0.022 g, 0.953 mmol) in approximately 5 mL of THF. The mixture was stirred for 20 min at room temperature until the cloudy grey suspension turned clear. To this sodium amalgam, a solution of [(^{Ph2PPr}PDI)FeBr][Br] (0.158 g, 0.191 mmol) in THF (~8 mL) was added. The color of the reaction mixture changed from purple to greenish brown within 15 h. After stirring for 48 h at room temperature, the reaction mixture was filtered through Celite to remove the byproduct

NaBr. The solvent was removed under vacuum to obtain 0.105 g (yield = 82%) of a greenish brown solid compound identified as (^{Ph2PPr}PDI)Fe. Anal. Cald. for $C_{39}H_{41}N_3FeP_2$: Cald. C, 69.96%; H, 6.17%; N, 6.28%. Found: C, 69.96%; H, 6.35%; N, 5.84%. ^{1}H NMR (400 MHz, benzene-d_6): 8.58 (d, J = 7.6 Hz, 2H, *phenyl*), 7.46 (t, J = 7.2 Hz, 5H, *phenyl*), 7.25 (t, J = 7.4 Hz, 4H, phenyl), 6.54 (dd, J = 16.1, 8.7 Hz, 7H, *phenyl*), 5.70 (t, J = 7.1 Hz, 3H, *phenyl*), 4.48 (d, J = 12.1 Hz, 2H, -CH_2), 3.44 (dd, J = 24.6, 12.5 Hz, 2H, -CH_2), 2.27 (dd, J = 9.1, 4.5 Hz, 4H, -CH_2), 2.19 (s, 6H, -CH_3), 1.68 (m, 2H, -CH_2). ^{13}C NMR (100.492 MHz, acetone-d_6, 25 °C): 144.64 (C=N), 133.23 (t, J = 6.7 Hz, *phenyl*), 131.81 (t, J = 4.7 Hz, *phenyl*), 127.44 (t, J = 4.5 Hz, *phenyl*), 126.08 (s, *phenyl*), 113.46 (s, *phenyl*), 113.27 (s, *phenyl*), 56.12 (s, -NCH$_2$CH$_2$), 28.95 (t, J = 8.7 Hz, -PCH$_2$CH$_2$), 28.00 (t, J = 3.15 Hz, -PCH$_2$$CH_2$), 14.99 (t, J = 1.0 Hz, CH$_3$). ^{31}P NMR (202.47 MHz, benzene-d_6, 25 °C): 69.87 (s, Fe-P).

Preparation of [(^{Ph2PPr}PDI)Co)][Cl] (4):

Under a nitrogen atmosphere, a 20 mL scintillation vial was charged with 0.400 g (0.682 mmol) of ^{Ph2PPr}PDI and approximately 5 mL of THF. A separate solution consisting of 0.575 g (0.652 mmol) $(Ph_3P)_3CoCl$ in approximately 5 mL THF was then added dropwise to the solution of ^{Ph2PPr}PDI. Upon addition, the solution immediately changed from yellow to a deep forest green color. The resulting reaction mixture was then capped and sealed under nitrogen and allowed to stir at 25 °C for 24 h. After stirring, the resulting deep green solution was filtered through a frit without Celite. The resulting THF insoluble solid was washed with 3x3 mL THF, 3x5 mL toluene, and 10 mL pentane and dried *in vacuo* to yield 0.345 g (0.499 mmol) of a deep green solid identified as [(^{Ph2PPr}PDI)Co][Cl] (yield = 77%). Recrystallization from a saturated solution of $CHCl_3$ at -35 °C afforded deep

green crystals. Anal. Cald. for $C_{39}H_{41}N_3CoP_2Cl$: Cald. C, 66.15%; H, 5.89%; N, 5.93%. Found: C, 55.54%; H, 4.69%; N, 4.89%.^{1}H NMR (400 MHz, acetone-d_6, 25 °C): 8.54 (d, J = 7.6 Hz, 2H, *phenyl*), 8.15 (t, J = 7.1 Hz, 1H, *phenyl*), 7.62 (t, J = 7.1 Hz, 4H, *phenyl*), 7.56 (t, J = 7.1 Hz, 2H, *phenyl*), 7.46 (d, J = 7.7 Hz, 4H, *phenyl*), 7.21 (t, J = 7.2 Hz, 2H, *phenyl*), 6.99 (t, J = 7.4 Hz, 4H, *phenyl*), 6.27 (d, J = 8.4 Hz, 4H, *phenyl*), 4.06 (d, J = 12.9 Hz, 2H, -CH_2), 3.62 (t, J = 6.5 Hz, 2H, -CH_2), 2.72 (t, J = 12.9 Hz, 2H, -CH_2), 2.60 (m, 2H, -CH_2), 2.38 (t, J = 4.7 Hz, 6H, -CH_3), 2.72 (m, 2H, -CH_2), 1.78 (m, 2H, -CH_2). ^{13}C NMR (100.492 MHz, acetone-d_6, 25 °C): 147.66 (*C*=N), 133.27 (t, J = 6.3 Hz, *phenyl*), 132.42 (t, J = 4.6 Hz, *phenyl*), 131.01 (s, *phenyl*), 130.68 (s, *phenyl*), 130.29 (t, J = 4.3 Hz, *phenyl*), 129.22 (t, J = 4.9 Hz, *phenyl*), 124.96 (t, *phenyl*), 54.49 (-N*C*$H_2$$CH_2$), 27.43 (-P$CH_2$*C*$H_2$), 15.40 (t, J = 2.9 Hz, -*C*H_3). ^{31}P NMR (202.47 MHz, acetone-d_6, 25 °C): 42.90 (s, Co-*P*).

Preparation of (^{Ph2PPr}PDI)Co (5):

Under a nitrogen atmosphere, a 20 mL scintillation vial was charged with 0.936 g of mercury (4.68 mmol) followed by freshly cut sodium (0.054 g, 2.34 mmol) in approximately 5 mL of THF. The mixture was stirred for 20 min at room temperature until the cloudy grey suspension turned clear. To this sodium amalgam mixture, a slurry solution of [(^{Ph2PPr}PDI)Co][Cl] (0.174 g, 0.234 mmol) in THF (~10 mL) was added. The color of the reaction mixture changed from green to deep red within 1 h. After stirring for 12 h at room temperature, the reaction mixture was filtered through Celite to remove the byproduct NaCl. The solvent was removed under vacuum to obtain 0.150 g (yield = 95 %) of a deep red solid identified as (^{Ph2PPr}PDI)Co. Recrystallization from a saturated solution of toluene at -35 °C afforded deep red crystals. Anal. Cald. for $C_{39}H_{41}N_3CoP_2$: Cald. C, 69.64%; H,

6.14%; N, 6.25%. Found: C, 68.82%; H, 5.94%; N, 5.89%. Magnetic susceptibility (Evans method, 25 °C): μ_{eff} = 1.6 μ_B. ^{1}H NMR (400 MHz, benzene-d_6, 25 °C): 73.31 (363.0 Hz), 65.14 (445.5 Hz), 56.24 (609.7 Hz), 11.52 (103 Hz), 10.86 (896.9 Hz), 9.81(912.9 Hz), 8.32(17.1 Hz), -0.48 (141.7 Hz), -3.28 (165.9 Hz), -9.12 (220.5 Hz), -26.63 (182.8 Hz).

Preparation of (^{Ph2PPr}PDI)Ni (6):

Under a nitrogen atmosphere, a 20 mL scintillation vial was charged with 0.0448 g (0.075 mmol) of ^{Ph2PPr}PDI and approximately 5 mL of toluene. A separate solution consisting of 0.021 g (0.076 mmol) of $Ni(COD)_2$ in approximately 5 mL of toluene was then added dropwise to the solution of ^{Ph2PPr}PDI. Upon addition, the solution immediately changed from the yellow color indicative of ^{Ph2PPr}PDI to a deep olive solution. The resulting reaction mixture was then capped and sealed under nitrogen and allowed to stir at 23 °C for 24 h. After stirring, the resulting deep olive solution was filtered through Celite and the toluene was removed *in vacuo* to yield a dark green solid identified as (^{Ph2PPr}PDI)Ni. Recrystallization from an ether/pentane solution afforded 0.0307 g (61%) of clear dark green crystals. Anal. Cald. for $C_{39}H_{41}N_3NiP_2$: Calcd. C, 69.66%; H, 6.15%; N, 6.25 %. Found: C, 69.51%; H, 6.40%; N, 4.75%. Magnetic susceptibility (Evans method, 23 °C): μ_{eff} = 1.3 μ_B. ^{1}H NMR (400 MHz, benzene-d_6, 23 °C): 23.48 (874.7 Hz), 12.69 (401.6 Hz), 4.91 (334.0 Hz), -4.48 (6260 Hz).

General procedure for hydrosilylation of benzaldehyde at 0.01 mol %:

In the glovebox, an ambient temperature neat solution of $PhSiH_3$ (2.39 mL, 19.4 mmol) and benzaldehyde (1.97 mL, 19.4 mmol) was added to a 20 mL scintillation vial containing 1.3 mg (0.0019 mmol) of catalyst. The resulting solution was stirred for 2 min and then

exposed to air to deactivate the catalyst. The colorless solution was filtered through Celite and a ^{1}H NMR spectrum was recorded to determine the percent conversion.

General procedure for hydrosilylation of acetophenone at 0.01 mol %:

In the glovebox, an ambient temperature neat solution of $PhSiH_3$ (3.49 mL, 29.9 mmol) and benzaldehyde (3.68 mL, 29.9 mmol) was added to a 20 mL scintillation vial containing 2.0 mg (0.0029 mmol) of catalyst. The resulting solution was stirred for 2 min and then exposed to air to deactivate the catalyst. The colorless solution was filtered through Celite and a ^{1}H NMR spectrum was recorded to determine the percent conversion.

General procedure for hydrosilylation of ketones at 0.1 mol %:

In the glovebox, an ambient temperature neat solution of $PhSiH_3$ (0.48 mL, 3.87 mmol) and acetophenone (0.45 mL, 3.87 mmol) was added to a 20 mL scintillation vial containing 2.6 mg (0.003 mmol) of complex **5**. The resulting red solution was stirred for 5 min and then exposed to air to deactivate the catalyst. The light-yellow solution was then filtered through Celite directly into an NMR tube.

CHAPTER 2 – AN IMINOPYRIDINE COBALT CATALYST FOR NITRILE DIHYDROBORATION AND NEW SYNTHETIC ROUTE FOR AMIDE FORMATION*

2.1 ABSTRACT

The catalytic hydrofunctionalization of unsaturated substrates is an attractive and atom-efficient route of preparing value-added products. There is considerable interest in base metal catalyst development for hydrosilylation and hydroboration reactions. Importantly, Si-C bonds are formed during silicone curing, while B–C bonds can be used in Suzuki-Miyaura coupling to generate new C–C bonds. Herein, a redox-active diimine ligand featuring ethylpyridine substituents, ^{PyEt}PDI, was added to $CoCl_2$. A six-coordinate dichloride salt, [(^{PyEt}PDI)CoCl][Cl], was obtained and thoroughly characterized. Single crystal X-ray diffraction revealed a high-spin Co(II) center having an octahedral geometry. Subsequent addition of 2 equiv. of $NaEt_3BH$ resulted in the formation of (κ^4-*N*,*N*,*N*,*N*-^{PyEt}IP^{CHMe}N^{EtPy})Co. ^{1}H NMR spectroscopy revealed a new methyl singlet upfield at -1.75 ppm that suggests one electron reduction of the iminopyridine chelate along with a new doublet at 1.89 ppm that is indicative of imine reduction to amine by a transient cobalt hydride species. Single crystal X-ray diffraction revealed a distorted square planar low-spin Co(II) complex. After isolation of (κ^4-*N*,*N*,*N*,*N*-^{PyEt}IP^{CHMe}N^{EtPy})Co, efforts to reduce nitriles using HBPin were performed and this catalyst was found to be active at ambient conditions with maximum TOF of 380 h^{-1} to generate the corresponding *N*,*N*-diborylamines. Lastly, the *N*,*N*-diborylamines were used for the synthesis of amides, without the use of an external coupling reagent, by adding carboxylic acids and heating to 120 °C in benzene.

---

*Parts of this chapter have been taken from Ghosh, C.; Kim, S.; Mena, M. R.; Kim, J.-H.; Pal, R.; Rock, C. L.; Groy, T. L.; Baik, M.-H.; Trovitch, R. J. *J. Am. Chem. Soc.* **2019**, *141*, 38, 15327–15337.

2.2 Introduction

Industrial catalysis has relied on the use of precious metals due to their stability under atmospheric conditions.[21,22,23] While effective, more sustainable methods have become a driving force for developing inexpensive alternatives using Earth-abundant [24,25,26] and main-group metals.[27,28,29] As a result, Fe,[30] Ni,[31] Co,[32], and Mn,[33] complexes have been utilized over the past two decades to catalyze the hydrofunctionalization of alkynes, alkenes, ketones, and nitriles. Hydrogenation, hydrosilylation, hydroamination, and hydroboration reactions have been relied on to generate functionalized organic compounds in an atom-economical fashion. The resulting value-added products are often employed in cross-coupling reactions.[34-35] Furthermore, nitrile reduction is interesting because the stable triple bond between N and C can be exploited to afford amine functionalities within larger molecules. The reduction can be achieved using stoichiometric main-group reductants, such as $LiAlH_4$ and $NaBH_4$, although selectivity and possible low yields of products make this less attractive.[36] Because of this, catalytic hydroboration has become a common method due to its selectivity for the preparation of unsaturated nitrogenous compounds.[37] As previously stated, noble-metals such as Ir and Rh have taken precedence over base metals due to their high activity and stability.[38] New catalysts have been reported that use magnesium,[39] molybdenum,[40] iron,[41] and frustrated Lewis pairs [42,43] for imine and nitrile hydroboration. Although novel, these systems usually demand long reaction times (24 – 72 h), high catalyst loadings (10 – 20 mol %), and high temperatures (80 – 120 °C) while offering low selectivity for specific unsaturated groups. To this end, a catalyst for nitrile and imine hydroboration at mild conditions was pursued.

2.3 Results and Discussion

Synthesis and Characterization of Cobalt Complexes

Previously reported ^{PyEt}PDI[44] (1.05 equiv.) was added to $CoCl_2$ and the mixture was heated to 95 °C in toluene. After 4 days, complete consumption of $CoCl_2$ was observed, resulting in the formation of an insoluble light-brown compound (Figure 2.1). ^{1}H NMR spectroscopy revealed that the compound exhibits resonances outside the diamagnetic region, suggesting that it is paramagnetic (Figure 2.2).

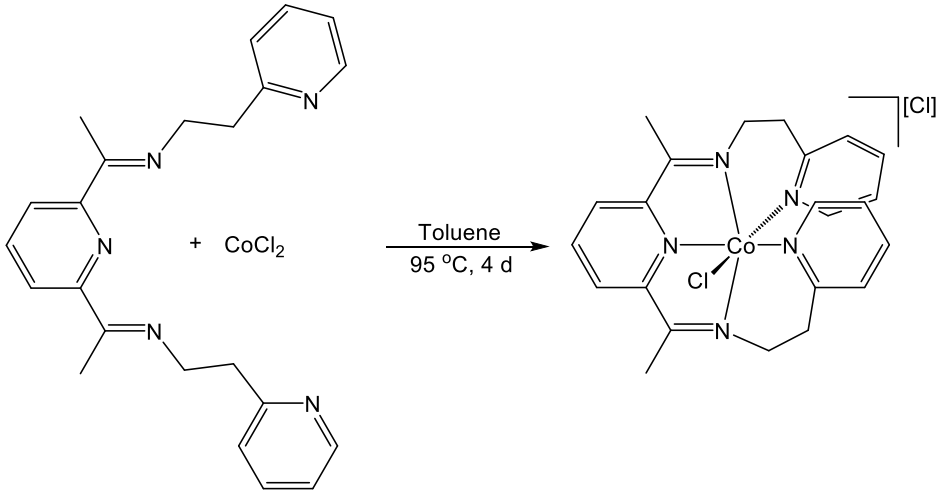

FIGURE 2.1. Synthesis of [(^{PyEt}PDI)CoCl][Cl] (**7**).

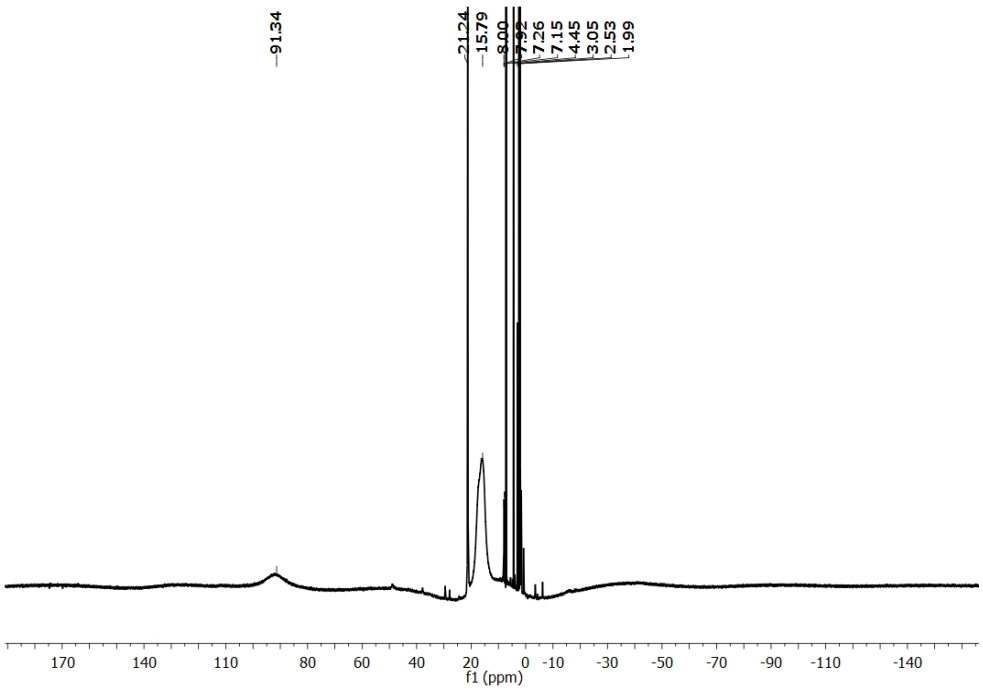

FIGURE 2.2 ^{1}H NMR of **7** in chloroform-*d* at 25 °C.

The paramagnetism of this product was confirmed by Evans method, which yielded a value of 3.8 μ_B at ambient temperature, consistent with a high-spin Co(II) – d^7 center in a pseudo-octahedral geometry.[45] Density functional theory (DFT) calculations supported this high-spin configuration, showing that high-spin **7** is 6.5 kcal/mol lower in energy than the low-spin configuration with only one unpaired electron on cobalt. Because PDI ligands can adopt a neutral, anionic, or dianionic state, several possible electronic structure alternatives were considered, but ligand reduction was not observed. Recrystallization in chloroform at -35 °C afforded a pseudo-octahedral coordination environment around the Co^{II} center. The bond lengths of N(1)–C(2) and N(3)–C(8) (1.271 and 1.284 Å, respectively) are consistent with a neutral PDI ligand.

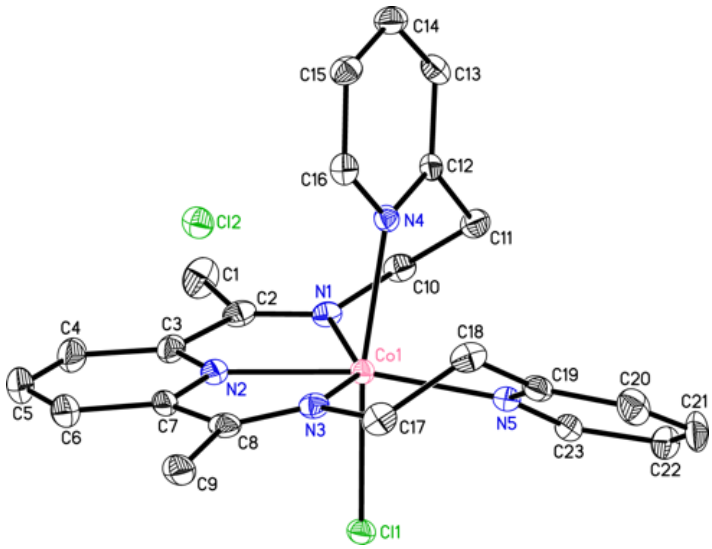

FIGURE 2.3. Solid state structure of **7** with 30% probability ellipsoids. Hydrogen atoms omitted for clarity.

TABLE 2.1. Selected bonds lengths (Å) for **7**.

	7 (Exp) (Å)	**7^{HS}(Calc)** (Å)	**7^{LS}(Calc)** (Å)
Co(1)–N(1)	2.173(4)	2.177	2.097
Co(1)–N(2)	2.072(4)	2.107	1.865
Co(1)–N(3)	2.155(4)	2.170	1.978
N(1)–C(2)	1.271(7)	1.282	1.289
C(2)–C(3)	1.489(8)	1.487	1.480
C(3)–N(2)	1.348(7)	1.334	1.339
N(2)–C(7)	1.331(7)	1.333	1.344
C(7)–C(8)	1.483(8)	1.487	1.476
C(8)–N(3)	1.284(7)	1.286	1.292

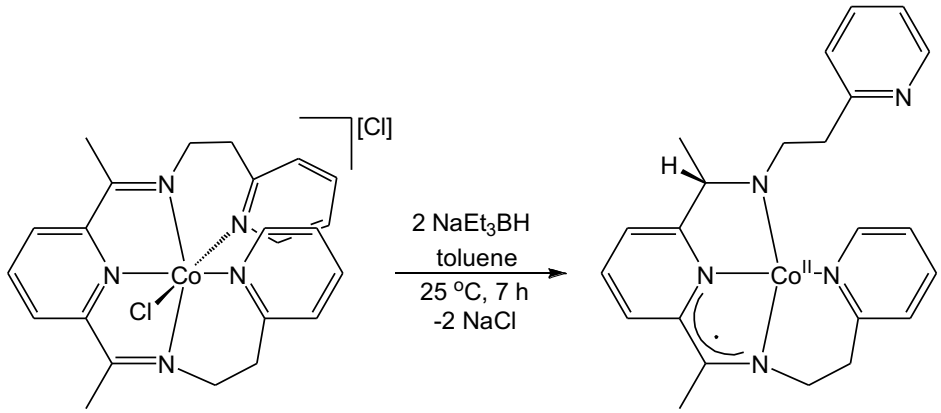

FIGURE 2.4. Synthesis of (κ^4-*N*,*N*,*N*,*N*-$^{PyEt}IP^{CHMe}N^{EtPy}$)Co (**8**).

To isolate a hydride complex, [(^{PyEt}PDI)CoCl][Cl] was treated with 2 equiv. of $NaEt_3BH$ in toluene, which afforded a forest green compound after stirring for 7 h at room temperature (Figure 2.4). The resulting product appeared to be diamagnetic based on NMR spectroscopic analysis (Figure 2.5). ^{1}H NMR spectroscopy revealed two methyl environments, one upfield-shifted singlet at −1.75 ppm and one doublet at 1.89 ppm. Furthermore, the appearance of 4 unique ^{1}H NMR resonances suggested a lack of C_2 symmetry. We anticipated a Co-hydride complex, although no hydride resonance was detected. Single crystals of **8** were obtained by Raja Pal by cooling a concentrated ether/pentane solution at −35 °C and single crystal X-ray diffraction revealed κ^4-*N*,*N*,*N*,*N*-chelate coordination around Co with one unbound pyridine arm (Figure 2.6). This unbound arm was a result of hydride migration to an imine carbon atom (consistent with a C(8)–N(3) single-bond distance of 1.473(4) Å, turning the formally neutral PDI chelate into an anionic imino(pyridine)amide ligand. Also, C(2)–C(3) distance of 1.409 Å is contracted and the N(1)–C(2) and N(2)–C(3) distances of 1.355 Å and 1.382 Å are elongated when compared to neutral imino(pyridal) lengths (which exhibit distances of 1.28, 1.35, and 1.47 Å, respectively),[46] suggesting a singly reduced chelate. The contracted Co(1)–N(4) bond

length of 1.914(2) Å is consistent with reported Co(II)−N amide distances,[47] and the bond angles of N(1)–Co(1)–N(2), N(1)–Co(1)–N(3), N(2)–Co(1)–N(3), and N(2)–Co(1)–N(4) were determined to be 82.11(11)°, 164.65(11)°, 84.12(11)°, and 169.30(11)°, respectively, giving rise to a distorted square-planar geometry around the Co(II) center.[48]

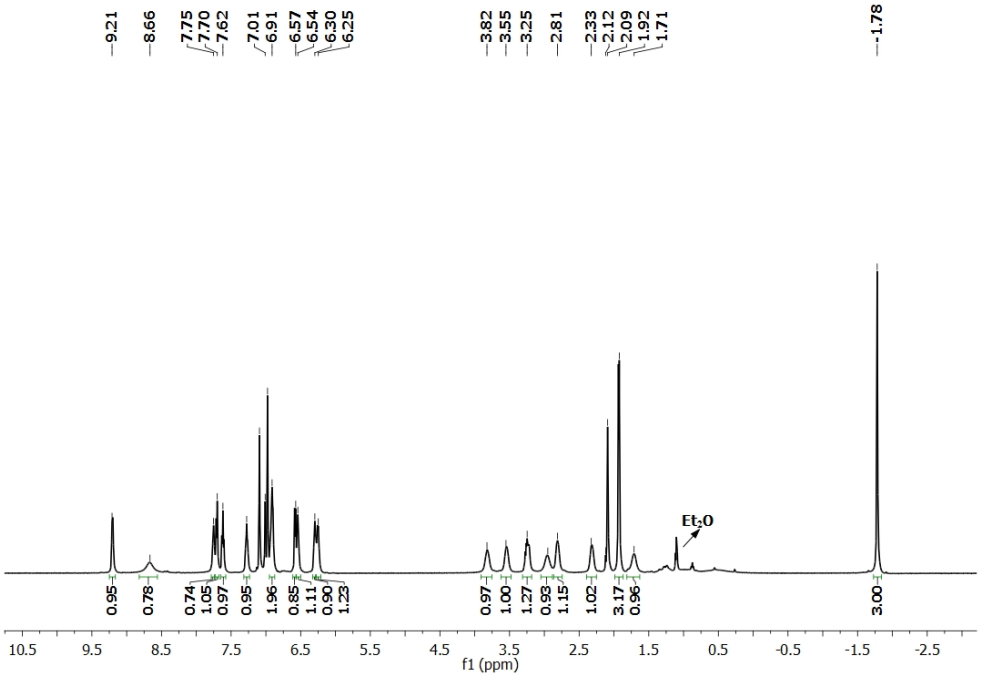

FIGURE 2.5. ^{1}H NMR spectrum of **8** in toluene-d_8 at 40 °C.

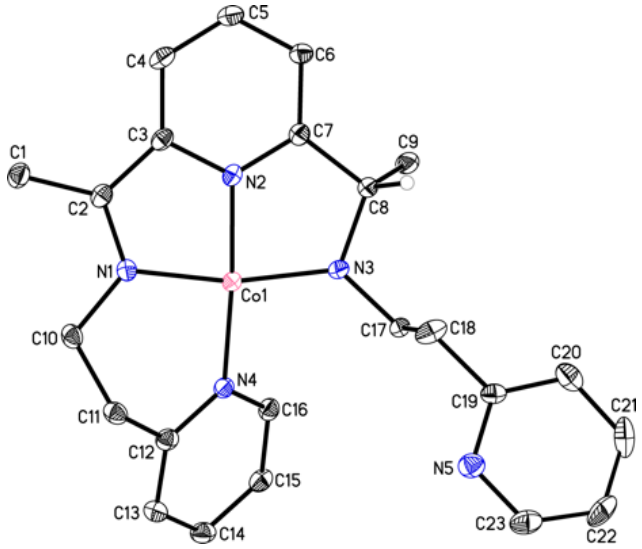

FIGURE 2.6. Solid state structure of **8** with 30% probability ellipsoids. Hydrogen atoms omitted for clarity.

TABLE 2.2. Nitrile dihydroboration using 1.0 mol% **8**.

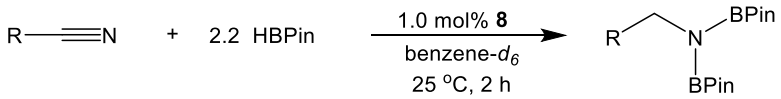

Product	% Conv.[a]	Isolated Yield%
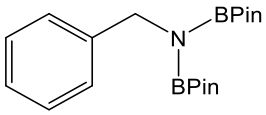	>99%	69%
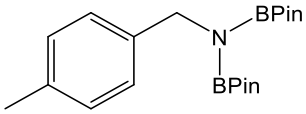	>99%	40%
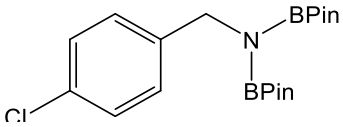	>99%	46%
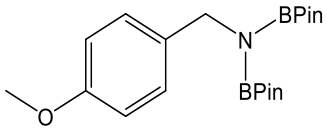	>99%	53%

[a]Percent conversion determined by ^{1}H NMR spectroscopy (integration of residual nitriles vs. diborylamine products).

2.4 Substrate Scope:

After isolation and characterization of **8**, this pre-catalyst was tested for nitrile dihydroboration activity. In our previous study,[49] 2.2 equiv. of HBPin was found to be an effective reductant for nitriles. A benzene-d_6 solution of benzonitrile and HBPin was added to 1.0 mol% of **8** in a J.Young tube and monitored by ^{1}H NMR spectroscopy for 2 h at room temperature. Remarkably, >99% conversion of the starting material to *N,N*-diborylamine was obtained, and this was duplicated on a larger scale and isolated (Table 2.2). Inspired by this result, with the help of a previous graduate student C. Ghosh, we tested

3 additional nitriles, and the respective *N,N*-diborylamine products were isolated via recrystallization from pentane or ether in modest yield (Table 2.2).

2.5 New Route for Amide Synthesis:

In 2015, Nikonov and co-workers discovered that reducing nitriles in the presence of a molybdenum catalyst and HBCat results in the formation of $PhCH_2N(BCat)_2$, which can react with benzaldehyde to produce the corresponding imine without the need for a dehydrating agent.[50] In 2019, Tobita and co-workers reported that boryl- and diborylamines can be cross-coupled to aryl bromides in the presence of excess KO^tbu and a catalytic quantity of $Pd(dba)_2$ and CyJohnPhos.[51] Organoborane reagents have emerged as effective coupling reagents for the amidation of carboxylic acids,[52] although direct amidation from functionalized borylamines was previously unreported. To this end, borylamines were evaluated as amide coupling reagents.

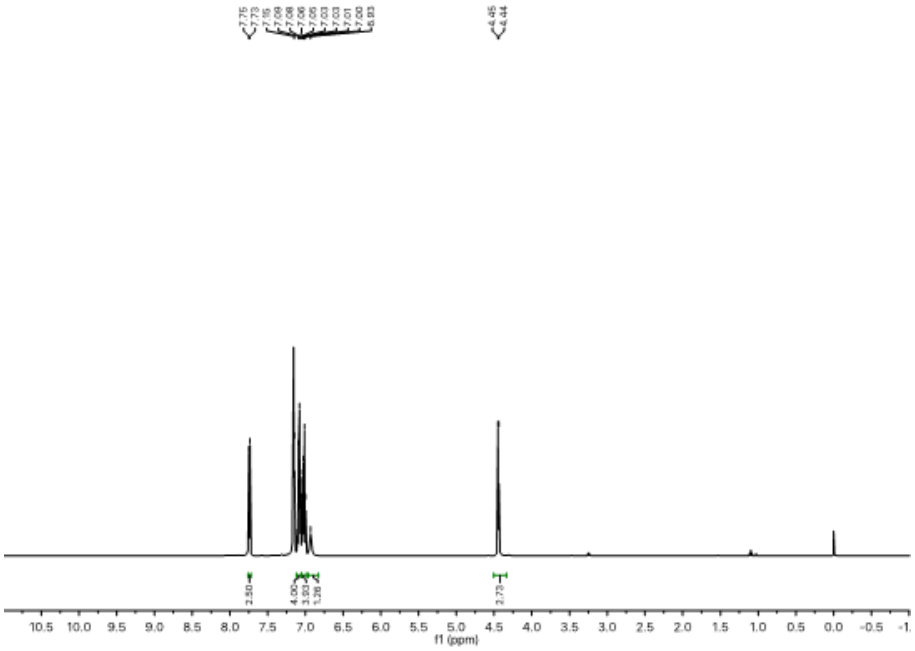

FIGURE 2.7 ^{1}H NMR spectrum of isolated $PhC(O)NHCH_2Ph$ in benzene-d_6 referenced to an internal TMS standard.

Heating a stoichiometric mixture of $PhCH_2N(BPin)_2$ and benzoic acid in benzene-d_6 to 120 °C in the absence of catalyst resulted in complete conversion to *N*-benzylbenzamide and $O(BPin)_2$ after 24 h. Recrystallization from warm benzene upon cooling to 3 °C yielded pure *N*-benzylbenzamide in modest yield as judged by ^{1}H NMR spectroscopy (Figure 2.7).

Functional groups associated with the borylamine (2a-2d) had no effect on amide synthesis when using benzoic acid in Table 2.3. The functional group tolerance of different acids was examined and 3-dimethylaminobenzoic acid and thizole-4-carboxylic acid (2e-2f) afforded the respective *N*-benzyl amide. While the substrate scope for this reaction has yet to be fully explored, a larger substrate scope, mechanistic studies, and optimization should be described in a forthcoming contribution.

TABLE 2.3. Coupling of *N*,*N*-diboryl amines and carboxylic acids to generate amides.

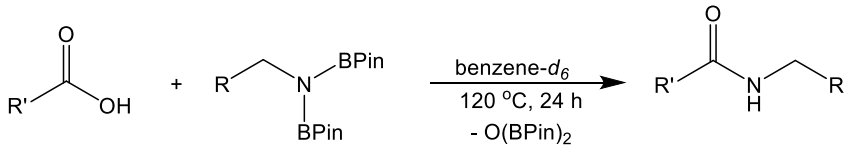

	Product	% Conv.[a]	Isolated Yield%
2a	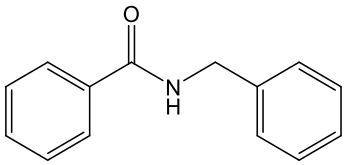	>99%	53%
2b	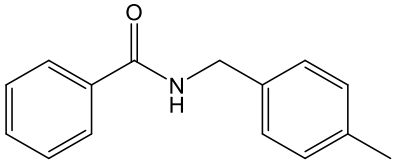	>99%	60%
2c	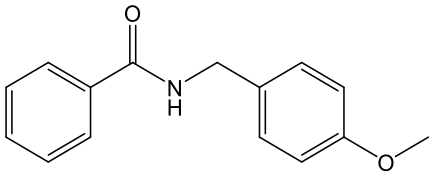	>99%	57%
2d	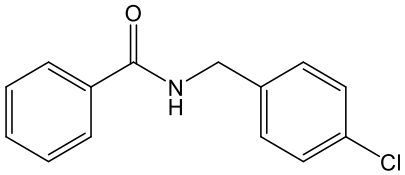	>99%	46%
2e	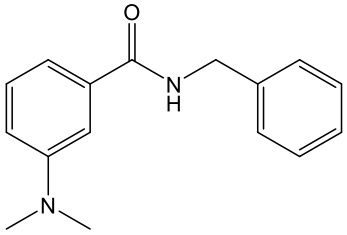	>99%	61%
2f	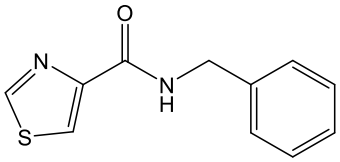	>99%	46%

[a]Percent conversion determined by ^{1}H NMR spectroscopy (integration of residual carboxylic acids/amines vs. amide products).

2.6 Conclusion

In conclusion, we demonstrated the nitrile hydroboration efficacy of a cobalt complex, (κ^4-*N*,*N*,*N*,*N*-$^{PyEt}IP^{CHMe}N^{EtPy}$)Co, that features a redox non-innocent ligand. This complex features a low-spin Co(II) center that antiferromagnetically couples to a ligand based radical. This facilitates nitrile dihydroboration catalysis at ambient temperature with turnover frequencies of up to 380 h^{-1}, the highest reported for this transformation.[53] In addition to nitrile reduction, we also demonstrated a new methodology of synthesizing amide without the use of coupling agents. Ultimately, the scope of amide formation has not been thoroughly explored, but its application can be exploited for further advances in the field of C–N bond coupling.

2.7 Experimental

General Considerations: All reactions were performed inside an MBraun glovebox under an atmosphere of purified nitrogen. Toluene, tetrahydrofuran, pentane, and diethyl ether were purchased from Sigma-Aldrich, purified using a Pure Process Technology solvent system, and stored in the glovebox over activated 4 Å molecular sieves and sodium before use. Benzene-d_6 and chloroform-*d* were purchased from Cambridge Isotope Laboratories and dried over 4 Å molecular sieves. 2,6-Diacetylpyridine, 2-(2-aminoethyl)pyridine, and benzonitrile were obtained from TCI America. 4-Methoxybenzonitrile, *p*-tolunitrile, 4-fluorobenzonitrile, 4-(trifluoromethyl)benzonitrile, 4-chlorobenzonitrile, 2-phenoxyacetonitrile, propionitrile, isobutyronitrile, benzoic acid, and 3-phenylpropanoic acid were obtained from Oakwood. Acetonitrile, 3-(dimethylamino)propionitrile, 4-acetylbenzonitrile, sodium triethylborohydride, pinacolborane, iodine, and

3-dimethylaminobenzoic acid were purchased from Sigma-Aldrich. Cobalt dichloride was obtained from Strem, while 2-furonitrile and thiazole-4-carboxylic acid were obtained from CombiBlocks. Propionitrile and isobutyronitrile were dried over CaH_2 and distilled prior to use, and all other liquid substrates were dried over 4 Å molecular sieves. 4-Fluorobenzonitrile was recrystallized from diethyl ether. Celite was purchased from Acros. The *N*,*N*-diborylamine products in Table 2.2 were isolated following recrystallization from diethyl ether under inert atmosphere because they decompose slowly in air. Solution ^{1}H NMR spectra were recorded at room temperature (40 °C for **8**) on a Varian 400-MR (400 MHz), Varian 500-MR (500 MHz), Bruker Ascend 400 MHz, or Bruker Ascend 500 MHz NMR spectrometer. All ^{1}H NMR and ^{13}C NMR chemical shifts are reported in parts per million relative to $Si(CH_3)_4$ using internal $Si(CH_3)_4$ or ^{1}H (residual) and ^{13}C chemical shifts of the solvent as secondary standards. ^{19}F NMR spectra are referenced to internal tetramethylsilane (TMS) through the proton channel. Elemental analyses were performed at Robertson Microlit Laboratories, Inc. (Ledgewood, NJ). Solution-state magnetic susceptibility was determined via the Evans method on the Varian 400 MHz spectrometer.

Preparation of [(^{PyEt}PDI)CoCl][Cl] (7): In a nitrogen-filled glovebox, a 100 mL thick-walled glass vessel was charged with $CoCl_2$ (1.166 g, 8.98 mmol) followed by ^{PyEt}PDI (3.50 g, 9.43 mmol) in ~30 mL of toluene. The apparatus was sealed, taken outside the box, and heated at 95 °C in a preheated oil bath. After stirring for 4 days, the reaction mixture was filtered through Celite using chloroform and the solvent was removed under vacuum. The residual light-brown solid was washed with pentane to remove unreacted ligand and then dried to yield 0.745 g (1.49 mmol, 17%) of a light-brown solid identified

as [(^{PyEt}PDI)CoCl][Cl]. Single crystals as a pentachloroform solvate were obtained upon cooling a concentrated $CHCl_3$ solution to −35 °C. Anal. Calcd. for $C_{23}H_{25}N_5Cl_2Co\cdot2(CHCl_3)$: C, 40.57%; H, 3.67%; N, 9.46%. Found C, 40.88%; H, 3.79%; N, 9.46%. Magnetic susceptibility (Evans method acetonitrile-d_3 solvent, 25 °C): μ_{eff} = 3.8 μ_B.^{1}H NMR (chloroform-*d*, 25 °C): 91.41 (3233 Hz), 21.02 (49 Hz), 16.35 (1491 Hz), 15.02 (1491 Hz).

Preparation of (κ^4-*N*,*N*,*N*,*N*-^{PyEt}IP^{CHMe}N^{EtPy})Co (8): In a nitrogen filled glovebox, a 100 mL round-bottom flask was filled with [(^{PyEt}PDI)CoCl][Cl] (99.9 mg, 0.1993 mmol) in ∼20 mL of toluene and cooled in a liquid nitrogen cooled cold well for 20 min. A 20 mL scintillation vial containing a 1.0 M solution of $NaEt_3BH$ (0.4 mL, 0.3985 mmol) in toluene was also cooled in the cold well for 20 min. Then, the $NaEt_3BH$ was added dropwise to the round-bottom flask containing the suspension of **7** in toluene. Initially, the color changed from light green to red and then to forest green color. After stirring for 7 h, the reaction mixture was filtered through Celite to remove the NaCl byproduct, and then the solvent was removed under vacuum. The residue was washed twice with pentane (3 mL each time) and then dried to obtain 64.5 mg (0.150 mmol, 75%) of a forest green solid identified as **8**. Single crystals were obtained by cooling a concentrated ether/pentane solution at −35 °C. Anal. Calcd. for $C_{23}H_{26}N_5Co$: C, 64.03%; H, 6.07%; N, 16.23%. Found: C, 63.62%; H, 6.28%; N, 15.86%. ^{1}H NMR (500 MHz, toluene-d_8, 40 °C): 9.20 (d, *J* = 6.4 Hz, 1H, *pyridyl*), 8.66 (br, 1H, *pyridyl*), 7.75 (m, 1H, *pyridyl*), 7.71 (d, *J* = 8.2 Hz, 1H, *pyridyl*), 7.62 (t, *J* = 7.5 Hz, 1H, *pyridyl*), 7.28 (t, *J* = 6.3 Hz, 1H, *pyridyl*), 6.91 (m, 2H, *pyridyl*), 6.58 (d, *J* = 7.6 Hz, 1H, *pyridyl*), 6.54 (m, 1H, *pyridyl*), 6.30 (m, 1H, *pyridyl*), 6.25 (m, 1H, −C*H*), 3.82 (br, 1H, −CH_2), 3.55 (br, 1H, −CH_2), 3.25 (br, 1H, − CH_2), 2.95

(br, 1H, − CH_2), 2.81 (br, 1H, − CH_2), 2.33 (br, 1H, − CH_2), 1.93 (d, J = 6.4 Hz, 3H, −CH_3), 1.71 (br, 1H,− CH_2), −1.78 (s, 3H, −CH_3). ^{13}C NMR (126 MHz, toluene-d_8, 40 °C): 178.71 (*C*≡N), 162.43 (*pyridyl*), 161.96 (*pyridyl*), 153.30 (*pyridyl*), 152.00 (*pyridyl*), 137.66 (*pyridyl*), 133.98 (*pyridyl*), 133.73 (*pyridyl*), 132.00 (*pyridyl*), 128.78 (*pyridyl*), 122.76 (*pyridyl*), 122.66 (*pyridyl*), 122.38 (*pyridyl*), 120.00 (*pyridyl*), 114.42 (*pyridyl*), 102.60 (*pyridyl*), 72.47 (−*C*H), 49.76 (−*C*H$_2$), 48.64 (−*C*H$_2$), 46.81 (−*C*H$_2$), 37.68 (−*C*H$_2$), 24.15 (−*C*H$_3$), 20.20 (−*C*H$_3$).

General Procedure (A) for the Hydroboration of Nitriles:

In the nitrogen filled glove box, a benzene-d_6 solution of benzonitrile (62.1 μL, 0.603 mmol) and pinacolborane (0.19 mL, 1.326 mmol) was added to a vial containing 2.6 mg (0.0060 mmol) of **8**. The resulting solution immediately changed color from green to dark purple, which was transferred to a J. Young tube and allowed to stand at ambient temperature for 2 h. Both ^{1}H NMR and ^{13}C NMR spectroscopy confirmed >99% conversion of the starting nitrile compound to diboryl amine, PhCH$_2$N(BPin)$_2$ after 2 h at room temperature. After removal of the solvent under vacuum, the product was recrystallized from pentane at -35 °C to obtain a white solid (0.150 g, 0.419 mmol, yield = 69%).

General Procedure (B) for Amide Synthesis:

In a nitrogen filled glove box, to a vial containing a benzene-d_6 solution of (PinB)$_2$NCH$_2$Ph (0.400 g, 1.117 mmol), benzoic acid (0.136 g, 1.117 mmol) was added. The pale-yellow solution was then removed from the glove box and set in a 120 °C oil bath for 24 h. No immediate color change occurred. Both ^{1}H NMR and ^{13}C NMR spectroscopy confirmed >99% conversion to the product, PhC(O)NHCH$_2$Ph, after 24 h. After removal of the

solvent under vacuum, the product was recrystallized from benzene at 3 °C to obtain a white crystalline solid (0.124 g, 0.588 mmol, yield = 53%).

Characterization of Isolated *N*,*N*-Diborylamines

Diborylation of benzonitrile: $PhCH_2N(BPin)_2$ was synthesized from benzonitrile using General Procedure A and isolated as a white solid in 69% yield (0.150 g). ^{1}H NMR (500 MHz, benzene-d_6): 7.60 (d, J = 7.2 Hz, 2H, *phenyl*), 7.26 (t, J = 7.7 Hz, 2H, *phenyl*), 7.12 (t, J = 7.4 Hz, 1H, *phenyl*), 4.63 (s, 2H, -CH_2), 1.04 (s, 24H, C(CH_3)$_2$). ^{13}C NMR (126 MHz, benzene-d_6): 144.44 (*phenyl*), 128.93 (*phenyl*), 127.23 (*phenyl*), 83.17 (-CH$_2$N), 48.52 (-C(CH$_3$)$_2$), 25.23 (-C(CH$_3$)$_2$).

Diborylation of 4-methyl benzonitrile: (4-MePh)$CH_2N(BPin)_2$ was synthesized from 4-methylbenzonitrile using General Procedure A and isolated as a white solid in 40% yield (0.091 g). ^{1}H NMR (500 MHz, benzene-d_6): 7.01 (d, J = 7.8 Hz, 2H, *phenyl*), 6.98 (d, J = 7.9 Hz, 2H, *phenyl*), 3.55 (s, 2H, N(CH_2)), 2.12 (s, 3H, -CH_3), 1.05 (s, 24H, -C(CH_3)$_2$). ^{13}C NMR (126 MHz, benzene-d_6): 141.38 (*phenyl*), 136.20 (*phenyl*), 129.56 (*phenyl*), 82.96 (-NCH$_2$), 48.07 (-C(CH$_3$)$_2$), 25.64 (-C(CH$_3$)$_2$), 21.65 (-CH$_3$).

Diborylation of 4-methoxybenzonitrile: (4-OMePh)$CH_2N(BPin)_2$ was synthesized from 4-methoxybenzonitrile using General Procedure A and isolated as a white solid in 46% yield (0.100 g). ^{1}H NMR (500 MHz, benzene-d_6): 7.58 (d, J = 8.7 Hz, 2H, *phenyl*), 6.88 (d, J = 8.7 Hz, 2H, *phenyl*), 4.61 (s, 2H, -NCH_2), 3.35 (s, 3H, -OCH_3), 1.06 (s, 24H, -C(CH_3)$_2$). ^{13}C NMR (126 MHz, benzene-d_6): 159.37 (*phenyl*), 136.54 (*phenyl*), 129.96 (*phenyl*), 114.34 (*phenyl*), 82.97 (-NCH$_2$), 55.36 (-C(CH$_3$)$_2$), 47.77 (-C(CH$_3$)$_2$), 25.21 (-OCH$_3$).

Diborylation of 4-chlorobenzonitrile: (4-ClPh)$CH_2N(BPin)_2$ was synthesized from 4-chlorobenzonitrile using General Procedure A and isolated as a white solid in 53% yield

(0.120 g). ^{1}H NMR (400 MHz, benzene-d_6): 7.35 (d, J = 8.0 Hz, 2H, *phenyl*), 7.19 (d, J = 8.1 Hz, 2H, *phenyl*), 4.46 (s, 2H, -NCH_2), 1.02 (s, 24H, -C(CH_3)$_2$). ^{13}C NMR (126 MHz, benzene-d_6): 142.82 (*phenyl*), 130.13 (*phenyl*), 129.08 (*phenyl*), 83.20 (-NCH$_2$), 47.69 (-C(CH$_3$)$_2$), 25.28 (-C(CH$_3$)$_2$).

Characterization of Isolated Amides:

Preparation of PhC(O)NHCH$_2$Ph: Compound 2a was synthesized from benzoic acid and (PinB)$_2$NCH$_2$Ph using General Procedure B and isolated as a white solid in 53% yield (0.124 g). ^{1}H NMR (500 MHz, benzene-d_6): 7.74 (d, J = 7.2 Hz, 2H, *phenyl*), 7.08 (m, 4H, *phenyl*), 7.01 (m, 4H, *phenyl*), 6.93 (s, 1H, -NH), 4.44 (d, J = 6.0 Hz, 2H, -CH_2). ^{13}C NMR (126 MHz, benzene-d_6): 166.84 (C=O), 139.14 (*phenyl*), 134.74 (*phenyl*), 130.90 (*phenyl*), 128.39 (phenyl), 128.17 (*phenyl*), 127.66 (*phenyl*), 127.28 (*phenyl*), 127.00 (*phenyl*), 43.61 (-CH$_2$).

Preparation of PhC(O)NHCH$_2$(4-Me-Ph): Compound 2b was synthesized from benzoic acid and (PinB)$_2$NCH$_2$(4-Me-Ph) using General Procedure B and isolated as a white solid in 60% yield (0.242 g). ^{1}H NMR (500 MHz, benzene-d_6): 7.59 (d, J = 7.7 Hz, 2H, *phenyl*), 7.09 (t, J = 16.1 Hz, 3H, *phenyl*), 7.02 (t, J = 15.1 Hz, 2H, *phenyl*), 6.94 (d, J = 7.7 Hz, 2H, *phenyl*), 5.82 (s, 1H, -NH), 4.45 (d, J = 5.7 Hz, 2H, CH_2), 2.10 (s, 3H, -CH_3). ^{13}C NMR (126 MHz, benzene-d_6): 166.20 (CO), 136.60 (*phenyl*), 136.08 (*phenyl*), 134.85 (*phenyl*), 130.79 (*phenyl*), 129.15 (*phenyl*), 128.21 (*phenyl*), 128.17 (*phenyl*) 127.06 (*phenyl*), 43.47 (-CH$_3$), 20.70 (-NHCH$_2$).

Preparation of PhC(O)NHCH$_2$(4-OMe-Ph): Compound 2c was synthesized from benzoic acid and (PinB)$_2$NCH$_2$(4-OMe-Ph) using General Procedure B and isolated as a white solid in 57% yield (0.214 g). ^{1}H NMR (500 MHz, benzene-d_6): 7.63 (d, J = 7.5 Hz,

2H, *phenyl*), 7.08 (t, J = 14.7 Hz, 3H, *phenyl*), 7.03 (t, J = 15 Hz, 2H, *phenyl*), 6.73 (d, J = 8.4 Hz, 2H, *phenyl*), 6.00 (s, 1H, -N*H*), 4.44 (d, J = 5.7 Hz, 2H, CH_2), 3.29 (s, 3H, -OCH_3). ^{13}C NMR (126 MHz, benzene-d_6): 166.80 (*C*O), 159.74 (*phenyl*), 135.46 (*phenyl*), 131.62 (*phenyl*), 131.36 (*phenyl*), 129.70 (*phenyl*), 128.74 (*phenyl*), 127.65 (*phenyl*), 114.52 (*phenyl*), 55.02 (-O*C*H_3), 43.77 (-NH*C*H_2).

Preparation of PhC(O)NHCH$_2$(4-Cl-Ph): Compound 2d was synthesized from benzoic acid and (PinB)$_2$NCH$_2$(4-Cl-Ph) using General Procedure B and isolated as a white solid in 46% yield (0.117 g). ^{1}H NMR (500 MHz, benzene-d_6): 7.60 (d, J = 7.7 Hz, 2H, *phenyl*), 7.10 (m, 1H, *phenyl*), 7.04 (m, 4H, *phenyl*), 6.82 (d, J = 8.1 Hz, 2H, *phenyl*), 5.82 (s, 1H, -N*H*), 4.22 (d, J = 5.6 Hz, 2H, CH_2). ^{13}C NMR (126 MHz, benzene-d_6): 166.31 (*C*O), 137.50 (*phenyl*), 134.55 (*phenyl*), 132.92 (*phenyl*), 131.04 (*phenyl*), 129.00 (*phenyl*), 128.52 (*phenyl*), 128.22 (*phenyl*), 127.05 (*phenyl*), 42.73 (-NH*C*H_2).

Preparation of 3-Me$_2$N-PhC(O)NHCH$_2$Ph: Compound 2e was synthesized from 3-dimethylaminobenzoic acid and (PinB)$_2$NCH$_2$Ph using General Procedure B and isolated as a white solid in 61% yield (0.136 g). ^{1}H NMR (400 MHz, benzene-d_6): 7.59 (s, 1H, *phenyl*), 7.18 (m, 2H, *phenyl*), 7.09 (m, 4H, *phenyl*), 7.00 (m, 1H, *phenyl*), 6.74 (s, 1H, -N*H*), 6.60 (d, 1H, *phenyl*), 4.50 (d, J = 5.9 Hz, 2H, -CH_2), 2.45 (s, 6H, N(CH_3)$_2$). ^{13}C NMR (126 MHz, benzene-d_6): 167.46 (*C*O), 150.68 (*phenyl*), 139.34 (*phenyl*), 135.72 (*phenyl*), 128.76 (*phenyl*), 128.38 (*phenyl*), 128.21 (*phenyl*), 128.09 (*phenyl*), 127.97 (*phenyl*), 126.95 (*phenyl*), 114.87 (*phenyl*), 114.13 (*phenyl*), 112.10 (*phenyl*), 42.63 (-NH*C*H_2), 39.62 (N(*C*H_3)$_2$).

Preparation of (4-thiazole)C(O)NHCH$_2$Ph: Compound 2f was synthesized from 4-thiazolecarboxylic acid and (PinB)$_2$NCH$_2$Ph using General Procedure B and isolated as a white solid in 46% yield (0.103 g). ^{1}H NMR (400 MHz, benzene-d_6): 7.86 (t, J = 2.0 Hz, 1H,

thiazole), 7.80 (t, J = 2.0 Hz, 1H, *thiazole*), 7.52 (br s, 1H, N*H*), 7.10 (m, 2H, *phenyl*), 7.05 (m, 3H, *phenyl*), 4.40 (d, J = 7.4 Hz, 2H, CH_2). ^{13}C NMR (126 MHz, benzene-d_6): 160.30 (*C*O), 152.28 (*thiazole*), 152.20 (*thiazole*), 151.73 (*thiazole*), 138.98 (*phenyl*), 128.48 (*phenyl*), 127.10 (*phenyl*), 122.97 (*phenyl*), 43.02 (*C*H_2).

REFERENCES

[1] Marciniec, B. *Hydrosilylation of carbon—carbon multiple bonds in organic synthesis. In: Hydrosilylation*. Dordrecht: Springer Netherlands; **2009**:87–123.

[2] Ojima, I.; Kogure, T. Reduction of carbonyl compounds via hydrosilylation. 4. Highly regioselective reductions of.alpha.,.beta.-unsaturated carbonyl compounds. *Organometallics* **1982**, *1*, 10, 1390–1399.

[3] Schneider, N.; Finger, M.; Haferkemper, C.; Bellemin-Laponnaz, S.; Hofmann, P.; Gade, L. H. Metal Silylenes Generated by Double Silicon–Hydrogen Activation: Key Intermediates in the Rhodium-Catalyzed Hydrosilylation of Ketones. *Angew. Chem., Int. Ed*. **2009**, *48*, 1609−1613.

[4] Gutsulyak, D. V.; Vyboishchikov, S. F.; Nikonov, G. I. Cationic Silane σ-Complexes of Ruthenium with Relevance to Catalysis. *J. Am. Chem. Soc*. **2010**, *132*, 5950−5951.

[5] Enthaler, S.; Junge, K.; Beller, M. Sustainable Metal Catalysis with Iron: From Rust to a Rising Star? *Angew. Chem., Int. Ed*. **2008**, *47*, 3317−3321.

[6] Plietker, B. *Iron Catalysis in Organic Chemistry: Reactions and Applications*; Wiley-VCH: Weinheim, Germany, 2008.

[7] Trovitch, R. J. The Emergence of Manganese-Based Carbonyl Hydrosilylation Catalysts. *Acc. Chem. Res*. **2017**, *50*, 11, 2842–2852.

[8] Johnson, C.; Albrecht, M. Triazolylidene Iron(II) Piano-Stool Complexes: Synthesis and Catalytic Hydrosilylation of Carbonyl Compounds. *Organometallics* **2017**, *36*, 2902−2913.

[9] Wei, Y.; Liu, S.; Mueller-Bunz, H.; Albrecht, M. Synthesis of Triazolylidene Nickel Complexes and Their Catalytic Application in Selective Aldehyde Hydrosilylation. *ACS Catal*. **2016**, *6*, 8192−8200.

[10] Sun, J.; Deng, L. Cobalt Complex-Catalyzed Hydrosilylation of Alkenes and Alkynes. *ACS Catal*. **2016**, *6*, 290−300.

[11] Sauer, D. C.; Wadepohl, H.; Gade, L. H. Cobalt Alkyl Complexes of a New Family of Chiral 1,3-Bis(2-pyridylimino)isoindolates and Their Application in Asymmetric Hydrosilylation. *Inorg. Chem*. **2012**, *51*, 12948–12958.

[12] Kobayashi, K.; Taguchi, D.; Moriuchi T.; Nakazawa H. Chemoselective Hydrosilylation of Olefin/Ketone Catalyzed by Iminobipyridine Fe and Co complexes. *ChemCatChem*. **2020**, *12*, 736-739.

[13] Verhoeven, D. G. A.; Kwakernaak, J.; van Wiggen, M. A. C.; Lutz, M.; Moret, M. E. Cobalt(II) and (I) Complexes of Diphosphine-Ketone Ligands: Catalytic Activity in Hydrosilylation Reactions. *Eur. J. Inorg. Chem*. **2019**, 660–667.

[14] Mukhopadhyay, T. K.; Flores, M.; Groy, T. L.; Trovitch, R. J. A Highly Active Manganese Precatalyst for the Hydrosilylation of Ketones and Esters. *J. Am. Chem. Soc*. **2014**, *136*, 3, 882–885.

[15] Mukhopadhyay, T. K.; Rock, C. L.; Hong, M.; Ashley, D. C.; Groy, T. L.; Baik, M.-H.; Trovitch, R. J. Mechanistic Investigation of Bis(imino)pyridine Manganese Catalyzed Carbonyl and Carboxylate Hydrosilylation. *J. Am. Chem. Soc*. **2017**, *139*, 4901–4915.

[16] Russell, S. K.; Bowman, A. C.; Lobkovsky, E.; Wieghardt, K.; Chirik, P. J. Synthesis and Electronic Structure of Reduced Bis(imino)pyridine Manganese Compounds. *Eur. J. Inorg. Chem*. **2012**, 535−545.

[17] Ben-Daat, H.; Hall, G. B.; Groy, T. L.; Trovitch, R. J. Rational Design of Rhodium Complexes Featuring κ^4-*N*,*N*,*N*,*N*- and κ^5-*N*,*N*,*N*,*P*,*P*-Bis(imino)pyridine Ligands. *Eur. J. Inorg. Chem*. **2013**, 4430−4442.

[18] Reed, B. R.; Stoian, S. A.; Lord, R. L.; Groysman, S. The aldimine effect in bis(imino)pyridine complexes: non-planar nickel(I) complexes of a bis(aldimino)pyridine ligand. *Chem. Commun.* **2015**, *51*, 6496−6499.

[19] Weil, J. A.; Bolton, J. R. *Electron Paramagnetic Resonance: Elementary Theory and Practical Applications*; John Wiley & Sons, **2007**.

[20] Stoll, S.; Schweiger, A. EasySpin, a Comprehensive Software Package for Spectral Simulation and Analysis in EPR. *J. Magn. Reson.* **2006**, *178*, 42–55.

CHAPTER 2

[21] Fagnou, K.; Lautens, M. Rhodium-Catalyzed Carbon−Carbon Bond Forming Reactions of Organometallic Compounds. *Chem. Rev*. **2003**, *103*, 169−196.

[22] Mkhalid, I. A. I.; Barnard, J. H.; Marder, T. B.; Murphy, J. M.; Hartwig, J. F. C−H Activation for the Construction of C−B Bonds. *Chem. Rev.* **2010**, *110*, 890−931.

[23] Johansson Seechurn, C. C. C.; Kitching, M. O.; Colacot, T. J.; Snieckus, V. Palladium-Catalyzed Cross-Coupling: A Historical Contextual Perspective to the 2010 Nobel Prize. *Angew. Chem., Int. Ed.* **2012**, *51*, 5062−5085.

[24] Cahiez, G.; Moyeux, A. Cobalt-Catalyzed Cross-Coupling Reactions. *Chem. Rev*. **2010**, *110*, 1435−1462.

[25] Gurung, S. K.; Thapa, S.; Kafle, A.; Dickie, D. A.; Giri, R. Copper-Catalyzed Suzuki–Miyaura Coupling of Arylboronate Esters: Transmetalation with (PN)CuF and Identification of Intermediates. *Org. Lett.* **2014**, *16*, 1264−1267.

[26] Dunetz, J. R.; Fandrick, D.; Federsel, H. J. Spotlight on Non-Precious Metal Catalysis. *Org. Process Res. Dev*. **2015**, *19*, 1325−1326.

[27] Revunova, K.; Nikonov, G. I. Main group catalysed reduction of unsaturated bonds. *Dalton Trans.* **2015**, *44*, 840−866.

[28] Buch, F.; Brettar, J.; Harder, S. Hydrosilylation of Alkenes with Early Main-Group Metal Catalysts. *Angew. Chem., Int. Ed*. **2006**, *45*, 2741−2745.

[29] Hill, M. S.; Liptrot, D. J.; Weetman, C. Alkaline earths as main group reagents in molecular catalysis. *Chem. Soc. Rev.* **2016**, *45*, 972−988.

[30] Blom, B.; Enthaler, S.; Inoue, S.; Irran, E.; Driess, M. Electron-Rich N-Heterocyclic Silylene (NHSi)–Iron Complexes: Synthesis, Structures, and Catalytic Ability of an Isolable Hydridosilylene–Iron Complex. *J. Am. Chem. Soc*. **2013**, *135*, 6703−6713.

[31] Porter, T. M.; Hall, G. B.; Groy, T. L.; Trovitch, R. J. Importance of co-donor field strength in the preparation of tetradentate α-diimine nickel hydrosilylation catalysts. *Dalton Trans*. **2013**, *42*, 14689−14692.

[32] Zhou, H.; Sun, H.; Zhang, S.; Li, X. Synthesis and Reactivity of a Hydrido CNC Pincer Cobalt(III) Complex and Its Application in Hydrosilylation of Aldehydes and Ketones. *Organometallics*, **2015**, *34*, 1479−1486.

[33] Gregg, B. T.; Hanna, P.K.; Crawford, E. J.; Cutler, A. R. Hydrosilation of manganese acyls $(CO)_5MnCOR$ (R = CH_3, Ph). *J. Am. Chem. Soc.* **1991**, *113*, 384.

[34] Nakao, Y.; Hiyama, T. Silicon-based cross-coupling reaction: an environmentally benign version. *Chem. Soc. Rev.* **2011**, *40*, 4893−4901.

[35] Torborg, C.; Beller, M. Recent Applications of Palladium-Catalyzed Coupling Reactions in the Pharmaceutical, Agrochemical, and Fine Chemical Industries. *Adv. Synth. Catal*. **2009**, *351*, 3027−3043.

[36] Colyer, J. T.; Andersen, N. G.; Tedrow, J. S.; Soukup, T. S.; Faul, M. M. Reversal of Diastereofacial Selectivity in Hydride Reductions of *N-tert*-Butanesulfinyl Imines. *J. Org. Chem*. **2006**, *71*, 6859−6862.

[37] Dorsey, A. D.; Barbarow, J. E.; Trauner, D. Reductive Cyclization of δ-Hydroxy Nitriles: A New Synthesis of Glycosylamines. *Org. Lett*. **2003**, *5*, 3237−3239.

[38] Zaidlewicz, M.; Wolan, A.; Budny, M. *Hydrometallation of C=C and C=C Bonds. Group 3*, 2nd ed.; Knochel, P., Molander, G. A., Eds.; Elsevier: Amsterdam, **2014**.

[39] Weetman, C.; Anker, M. D.; Arrowsmith, M.; Hill, M. S.; Kociok-Köhn, G.; Liptrot, D. J.; Mahon, M. F. Magnesium-catalysed nitrile hydroboration. *Chem. Sci*. **2016**, *7*, 628−641.

[40] Khalimon, A. Y.; Farha, P.; Kuzmina, L. G.; Nikonov, G. I. Catalytic hydroboration by an imido-hydrido complex of Mo(IV). *Chem. Commun*. **2012**, *48*, 455−457.

[41] Ruddy, A. J.; Kelly, C. M.; Crawford, S. M.; Wheaton, C. A.; Sydora, O. L.; Small, B. L.; Stradiotto, M.; Turculet, L. (*N*-Phosphinoamidinate)Iron Pre-Catalysts for the Room Temperature Hydrosilylation of Carbonyl Compounds with Broad Substrate Scope at Low Loadings. *Organometallics* **2013**, *32*, 5581−5588.

[42] Stephan, D. W.; Erker, G. Frustrated Lewis Pairs: Metal-free Hydrogen Activation and More. *Angew. Chem., Int. Ed*. **2010**, *49*, 46−76.

[43] Stephan, D. W.; Erker, G. Frustrated Lewis Pair Chemistry: Development and Perspectives. *Angew. Chem., Int. Ed*. **2015**, *54*, 6400−6441.

[44] Chiericato, G.; Arana, C. R.; Casado, C.; Cuadrado, I.; Abruña, H. D. Electrocatalytic reduction of carbon dioxide mediated by transition metal complexes with terdentate ligands derived from diacetylpyridine. *Inorg. Chim. Acta* **2000**, *300−302*, 32−42.

[45] Small, B. L.; Brookhart, M.; Bennett, A. M. A. Highly Active Iron and Cobalt Catalysts for the Polymerization of Ethylene. *J. Am. Chem. Soc*. **1998**, *120*, 4049−4050.

[46] Lu, C. C.; Weyhermüller, T.; Bill, E.; Wieghardt, K. Accessing the Different Redox States of α-Iminopyridines within Cobalt Complexes. *Inorg. Chem*. **2009**, *48*, 6055−6064.

[47] Lee, H. K.; Lam, C. H.; Li, S. L.; Zhang, Z. Y.; Mak, T. C. Low-Valent Chemistry of Cobalt Amide. Synthesis and Structural Characterization of Cobalt(II) Amido, Aryloxide, and Thiolate Compounds. *Inorg. Chem*. **2001**, *40*, 4691−4695.

[48] Goodwin, H. A. *Spin Crossover in Cobalt(II) Systems. In Spin Crossover in Transition Metal Compounds II*; Gütlich, P., Goodwin, H. A., Eds.; Springer: Berlin/Heidelberg, **2004**; pp 23−47.

[49] Ben-Daat, H.; Rock, C. L.; Flores, M.; Groy, T. L.; Bowman, A. C.; Trovitch, R. J. Hydroboration of alkynes and nitriles using an α-diimine cobalt hydride catalyst. *Chem. Commun*. **2017**, *53*, 7333−7336.

[50] Khalimon, A. Y.; Farha, P. M.; Nikonov, G. I. Imido−Hydrido Complexes of Mo(IV): Catalysis and Mechanistic Aspects of Hydroboration Reactions. *Dalton Trans*. **2015**, *44*, 18945−18956.

[51] Kitano, T.; Komuro, T.; Tobita, H. Double and Single Hydroboration of Nitriles Catalyzed by a Ruthenium−Bis(silyl)-xanthene Complex: Application to One-Pot Synthesis of Diarylamines and N-Arylimines. *Organometallics*, **2019**, *38*, 1417−1420.

[52] Figueiredo, R. M.; Suppo, -S. J.; Campagne, -M. J. Nonclassical Routes for Amide Bond Formation. *Chem. Rev*. **2016**, *116*, 12029−12122.

[53] Ghosh, C.; Kim, S.; Mena, M. R.; Kim, J.-H.; Pal, R.; Rock, C. L.; Groy, T. L.; Baik, M.-H.; Trovitch, R. J. Efficient Cobalt Catalyst for Ambient-Temperature Nitrile Dihydroboration, the Elucidation of a Chelate-Assisted Borylation Mechanism, and a New Synthetic Route to Amides. *J. Am. Chem. Soc*. **2019**, *141*, 38, 15327–15337.

APPENDIX A

PUBLISHED PORTIONS

Chapter 2 was published in the article referenced below.

Ghosh, C.; Kim, S.; Mena, M. R.; Kim, J.-H.; Pal, R.; Rock, C. L.; Groy, T. L.; Baik, M.-H.; Trovitch, R. J. Efficient Cobalt Catalyst for Ambient-Temperature Nitrile Dihydroboration, the Elucidation of a Chelate-Assisted Borylation Mechanism, and a New Synthetic Route to Amides. *J. Am. Chem. Soc*. **2019**, *141*, 38, 15327–15337.